J. Fluid Mech. (1993), *vol.* 257, *pp.* 33–63

Effects of imposed spanwise perturbations on plane mixing-layer structure

By JAMES H. BELL[1,2] AND RABINDRA D. MEHTA[2,3]

[1] Center for Turbulence Research, Stanford University/NASA Ames Research Center, USA

[2] Fluid Mechanics Laboratory, NASA Ames Research Center, Moffett Field, CA 94035-1000, USA

[3] Department of Aeronautics and Astronautics, JIAA, Stanford University, Stanford, CA 94305, USA

(Received 17 December 1992 and in revised form 12 May 1993)

The origin and evolution of spatially stationary streamwise vortical structures in plane mixing layers with laminar initial boundary layers were recently examined quantitatively (Bell & Mehta 1992). When both initial boundary layers were made turbulent, such spatially-stationary streamwise structures were *not* measured which is indicative of the high sensitivity of these structures to initial conditions. In the present study, the effects of four different types of spanwise perturbations at the origin of the mixing layer were investigated. The wavelengths of the imposed perturbations were chosen to be comparable to the initial Kelvin–Helmholtz wavelength. For the first two perturbations, the boundary layers were otherwise left undisturbed. A serration on the splitter plate trailing edge was found to have a relatively small effect on the formation and development of the streamwise structures. The introduction of cylindrical pegs in the high-speed side boundary layer not only generated a regular array of vortex pairs, but also affected the mixing-layer growth rate and turbulence properties in the far-field region. For the other two perturbations, the initial boundary layers were tripped on the splitter plate. An array of vortex generators mounted in the high-speed boundary layer and a corrugated surface attached to the splitter plate trailing edge had essentially the same effects. Both imposed a regular array of relatively strong streamwise vortices in counter-rotating pairs upon the mixing layer. This resulted in large spanwise distortions of the mixing layer mean properties and Reynolds stresses. While the vorticity injection increased the growth rate in the near-field region as expected, the far-field growth rate was reduced by a factor of about two, together with the peak Reynolds stress levels. This result is attributed to the effect of the relatively strong streamwise vorticity in making the spanwise structures more three-dimensional and hence reducing entrainment during the pairing process. The imposed streamwise vorticity did not follow the pattern of increasing spanwise spacing seen in the 'naturally occurring' streamwise vorticity. The mean streamwise vorticity decayed with increasing streamwise distance in all cases, albeit at different rates.

1. Introduction

Since turbulent mixing layers are commonly encountered in practice (e.g. flow reactors, combustion chambers and jet engines), the ability to control their structure, growth and mixing properties would obviously have a vital impact on many engineering applications. As a result, mixing layers have been a popular topic of study over the years in both experimental and computational investigations.

Flow visualization studies conducted in the late 1970s began to show that the near-field development of plane mixing layers was not only influenced by the formation and interaction of large-scale spanwise vortices (Brown & Roshko 1974), but also by the formation of a secondary structure which took the form of pairs of counter-rotating streamwise vortices (Konrad 1976; Bernal & Roshko 1986; Lasheras, Cho & Maxworthy 1986). The results suggested that the streamwise vortices first formed in the *braid* region connecting adjacent spanwise vortices, with their location determined by the strength and position of upstream disturbances. The results of Konrad (1976) and Bernal & Roshko (1986) also suggested that the scale, and hence spacing, of the streamwise vortices increased with downstream distance. Jimenez (1983) obtained time-averaged velocity measurements which showed strong spanwise 'wrinkles', thus confirming earlier conjecture that the streamwise structures were spatially stationary. The more detailed velocity measurements of Huang & Ho (1990) indicated that the spanwise spacing of the streamwise structures doubled after each of the first two pairings of the primary spanwise vortices that were investigated.

The presence and role of these 'naturally occurring' streamwise structures were recently investigated through detailed (time-averaged) measurements of the mean velocities and Reynolds stresses by Bell & Mehta (1989*a*, 1992). A plane, two-stream mixing layer was generated at a relatively high Reynolds number ($Re_\delta \approx 2.9 \times 10^4$), with a fixed velocity ratio, $(U_1 - U_2)/(U_1 + U_2) = 0.25$, and laminar initial boundary layers which were nominally two-dimensional. Measurements of the mean streamwise vorticity indicated that concentrated streamwise vortices were formed just downstream of the first spanwise roll-up. The initial average peak vorticity of these structures was equivalent to about 30% of the initial spanwise vorticity, and the average streamwise circulation was about 10% of the spanwise circulation. The streamwise vortices first appeared in clusters containing vorticity of both signs with their locations approximately consistent with those of weak incoming disturbances. Further downstream, the clusters re-organized to form an array of counter-rotating pairs. The wavelength associated with the streamwise vortices was found to increase, scaling approximately with the mixing-layer vorticity thickness. The vortices also weakened with downstream distance, the maximum mean vorticity decaying as approximately $1/X^{1.5}$. The mean streamwise vorticity was found to be strongly correlated in position, strength and scale with the secondary shear stress ($\overline{u'w'}$). The $\overline{u'w'}$ data suggested that the streamwise structures persisted through to what would normally be defined as the self-similar region, although they were very weak by this point and the mixing layer otherwise appeared to be nominally two-dimensional. In contrast, in the same mixing layer developing from tripped initial boundary layers, spatially stationary streamwise vortices were not observed and the far-field growth rate was about 25% lower than that for the layer with laminar initial boundary layers (Bell & Mehta 1990).

The streamwise structure that forms in undisturbed mixing layers is characterized by an irregular distribution of vortices. In order to gain a better understanding of the origin and evolution of these structures, some experimental studies have used spanwise triggering mechanisms to generate a regular array of streamwise vortices in the mixing layer. Breidenthal (1980) made the first attempt to modify the streamwise structure by installing wedges at regular intervals along the splitter plate trailing edge. His flow visualization results showed that the mixing layer rapidly formed the characteristic two-dimensional spanwise vortex structures and that further downstream all signs of the initial perturbation disappeared. Lasheras *et al.* (1986) perturbed the mixing layer by placing a small cylinder in one of the initial boundary layers and found that the generated horseshoe vortex induced the formation of streamwise vorticity on either

side, under the action of the strain produced by the spanwise vortices. Further downstream, the structure continued to propagate laterally through self-induction. Lasheras & Choi (1988) explored the effects of two types of sinusoidal perturbations in the form of indented and corrugated splitter plate trailing edges. They concluded that weak streamwise vorticity in the braid region was stretched under the positive strain generated by the spanwise vortices and this led to the formation of vortices whose axes were aligned with the direction of maximum strain. During the formation of the streamwise vortices, the spanwise vortices were found to maintain their two-dimensionality, thus indicating very little interaction between the two structures. However, further downstream, an undulation of the spanwise vortex cores was observed, with the same wavelength as the streamwise structures, but out of phase with what would be expected. Several disturbance wavelengths, centring around the initial Kelvin–Helmholtz wavelength, were investigated, but an optimum wavelength for maximum amplification was not observed. More recently, Nygaard & Glezer (1990, 1991) excited the spanwise vortex core instability using a time-harmonic waveform synthesized by a mosaic of surface film heaters, flush mounted on the splitter plate. They found that the streamwise vortices formed upstream of the first spanwise roll-up and almost any excitable wavelength would lead to their generation. If the spanwise excitation wavelength exceeded the initial Kelvin–Helmholtz wavelength, the primary vortices developed spanwise undulations associated with the core instability.

All the investigations on imposed spanwise perturbations described above were performed on relatively low Reynolds number ($Re_\delta < 3 \times 10^3$) mixing layers generated in water tunnels and the measurements were typically restricted to the near-field region of their development. One of the objectives of the present study was to try and regularize the streamwise vortex array generated in a relatively high Reynolds number ($Re_\delta \approx 2.5 \times 10^4$) mixing layer developing from laminar boundary layers. Another objective was to investigate the effects of relatively strong injected streamwise vorticity on the structure and development of a mixing layer originating from turbulent boundary layers. In particular, the effect of the vorticity injection on mixing-layer growth was to be investigated and the behaviour of the vorticity itself was to be compared to that occurring 'naturally' in the undisturbed case.

2. Experimental apparatus and techniques

The experiments were conducted in a mixing-layer wind tunnel (figure 1), consisting of two separate legs which are driven individually by centrifugal blowers connected to variable speed motors (Bell & Mehta 1989*b*). The two streams are allowed to merge at the sharp edge of the tapered splitter plate. The included angle at the splitter plate edge, which extends 15 cm into the test section, is about 1°. The test section is 36 cm in the cross-stream direction, 91 cm in the spanwise direction and 366 cm in length. One sidewall is slotted for probe access and flexible for pressure gradient control. For all the present measurements, the flexible wall was adjusted to give a nominally zero streamwise pressure gradient.

In the present study, the leg driven by the bigger blower was operated at a free-stream velocity in the test section, U_1, of 15 m/s while the flow speed in the other leg, U_2, was set at 9 m/s, thus giving a mixing layer with velocity ratio, $\lambda = (U_1 - U_2)/(U_1 + U_2) = 0.25$ ($r = U_2/U_1 = 0.6$). At these operating conditions, the measured streamwise turbulence level (u'/U_e) was about 0.15% and the transverse levels (v'/U_e and w'/U_e) were about 0.05%. The mean core-flow was found to be uniform to within 0.5% and cross-flow angles were less than 0.25°.

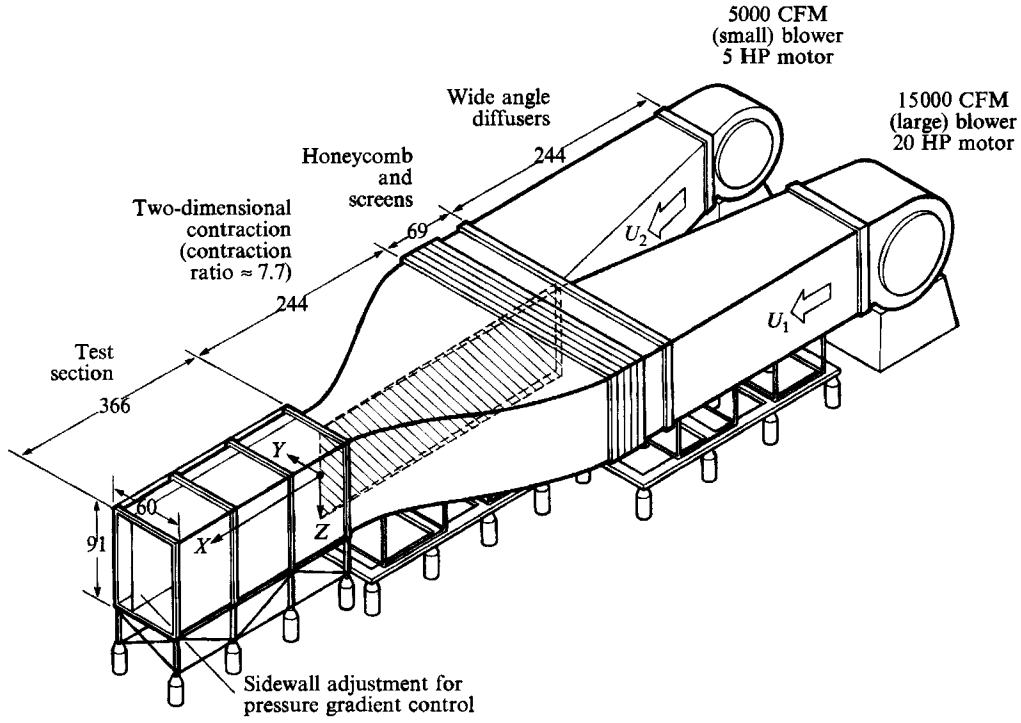

FIGURE 1. Schematic of mixing-layer wind tunnel. (All dimensions in cm.)

Condition	U (m/s)	δ_{99} (cm)	θ (cm)	Re_θ	H
High-speed side, undisturbed	15.0	0.40	0.053	525	2.52
Low-speed side, undisturbed	9.0	0.44	0.061	362	2.24
High-speed side, tripped	15.0	0.76	0.082	804	1.49
Low-speed side, tripped	9.0	0.85	0.094	567	1.50

TABLE 1. Initial boundary layer properties

For the first two spanwise perturbations described below, the boundary layers were otherwise left undisturbed, whereas for the last two perturbations the boundary layers were tripped in addition. For the tripped cases, the boundary layers on the splitter plate were perturbed using round-wire trips, of 0.8 mm diameter on the high-speed side and 1.2 mm diameter on the low-speed side. The trips were installed 15 cm upstream of the trailing edge to allow for the boundary layers to recover from the perturbation. Details of the boundary layers (without vorticity injection) measured at the splitter plate trailing edge are summarized in table 1.

The perturbation in the first experiment was a serration in the form of a sinusoidal variation in the splitter plate trailing edge in the (X, Z)-plane (figure 2*a*). The serration was similar to that used by Lasheras & Choi (1988) and was intended to introduce a small but regular spanwise variation in the mixing-layer origin, which would in turn induce the formation of streamwise vortices at regular intervals. In effect, the spanwise vortex lines are kinked in the (X, Z)-plane, thus producing a streamwise component of vorticity which is then stretched in the braid region. It was hoped that the resulting

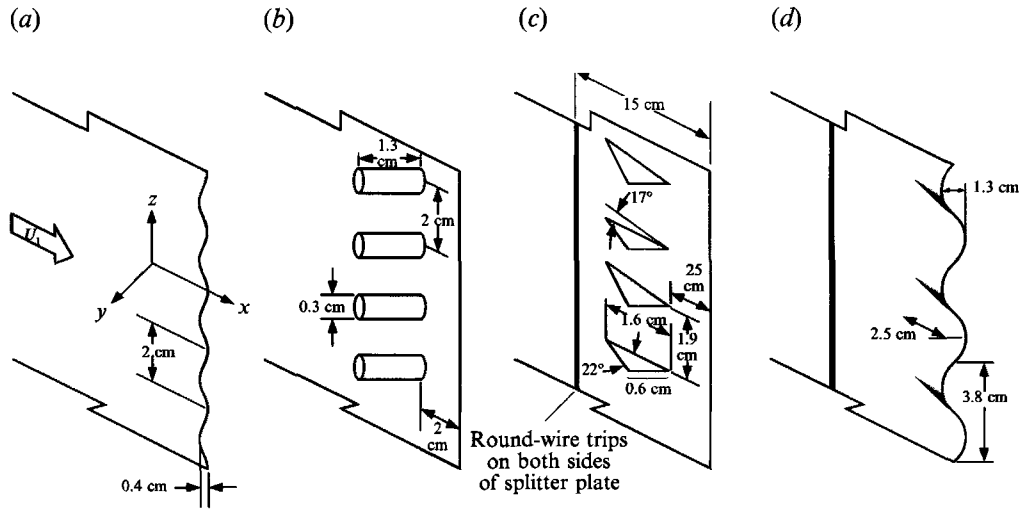

FIGURE 2. Schematic of perturbation mechanisms. (*a*) Serration; (*b*) pegs; (*c*) vortex generators; (*d*) corrugation.

vorticity field would display a behaviour similar to that in the 'natural' case, but with a more regular structure. The serration wavelength was chosen to be approximately equal to the initial Kelvin–Helmholtz wavelength of the spanwise vortices (~ 1.7 cm) and the amplitude was equivalent to 50 % of the combined boundary-layer thicknesses. Following Lasheras & Choi (1988), a relatively small amplitude was chosen so as to impose only a weak perturbation on the flow.

The second perturbation consisted of a single row of small cylindrical pegs installed within the high-speed side boundary layer on the splitter plate (figure 2*b*). The pegs protruded through the high-speed side boundary layer and, through interaction with the boundary layer, each peg produced a horse-shoe vortex with two legs of opposite-signed vorticity. The intention was to provide a regular array of streamwise vortices which would then presumably evolve in the mixing layer in the same way as the 'naturally-occurring' vorticity. The peg spacing was again comparable to the initial Kelvin–Helmholtz wavelength.

In the final two cases, perturbations were introduced in mixing layers originating from turbulent initial boundary layers in an attempt to impose a streamwise vortex structure which would otherwise be absent.

In the first case, streamwise vortices were generated by a row of half-delta wing vortex generators placed on the high-speed side of the splitter plate (figure 2*c*). The vortex generators were installed at alternating positive and negative angles of attack so as to produce an evenly-spaced row of counter-rotating streamwise vortices. The vortex generator spacing was comparable to the estimated initial Kelvin–Helmholtz wavelength, and the semi-span was approximately equal to the local boundary-layer thickness.

In the second case, an extension, corrugated in the cross-stream (Y) direction, was attached to the end of the splitter plate, thus giving it a three-dimensional trailing edge (figure 2*d*) – this perturbation is also similar to that investigated by Lasheras & Choi (1988). The corrugation induced vertical and lateral velocity components in the boundary layer such that the flow migrated towards the local trough (Eckerle, Sheibani & Awad 1992). The opposite effect took place in the other boundary layer and the secondary flow thus generated rolled-up into a streamwise vortex. Each full cycle of the

corrugation produced a pair of opposite-signed streamwise vortices and so the wavelength was chosen to equal roughly twice the Kelvin–Helmholtz wavelength; the amplitude was approximately equal to 0.8 times the sum of the boundary-layer thicknesses.

The wavelength associated with the generated streamwise vortices in all cases in the present study was equivalent to between one and two times the initial Kelvin–Helmholtz wavelength. The perturbation wavelength was not systematically varied in any of the present studies since previous experimental investigations (Lasheras & Choi 1988; Nygaard & Glezer 1991) have shown that virtually any wavelength can be successfully generated. This observation is consistent with results of stability analyses (Pierrehumbert & Widnall 1982; Rogers & Moser 1993*a*) which suggest that the mixing layer will amplify spanwise disturbances over a broad range of wavelengths, with the most-amplified wavelength being about $\frac{2}{3}$ of the Kelvin–Helmholtz wavelength.

Measurements were made using a rotatable cross-wire probe held on a three-dimensional traverse and linked to a fully automated data acquisition and reduction system controlled by a MicroVax II computer. The cross-wire probe had 5 μm diameter tungsten sensing elements about 1 mm long and positioned about 1 mm apart. The probe was calibrated statically in the potential core of the flow assuming a 'cosine-law' response to yaw, with the effective angle determined by calibration. The analog signals were filtered (low pass at 30 kHz), d.c. offset, and amplified ($\times 10$) before being fed into a computer interface. The interface contained a fast sample-and-hold A/D converter with 12 bit resolution and a multiplexer for connection to the computer. Individual statistics were averaged over 5000 samples obtained at a rate of between 400 and 2500 samples per second – note that this relatively low sampling rate does not affect the time-averaged data presented exclusively in this article.

Data were obtained in the (uv)- and (uw)-planes at eight streamwise stations within the test section, located from $X \approx 8$ to 250 cm downstream of the splitter plate. At each station, data were obtained in a cross-sectional plane which typically extended over 20 points in the cross-stream direction, and 60 points in the spanwise direction. The spanwise extent of the data set ranged from three to ten mixing-layer thicknesses, depending on the streamwise location. All the global properties presented in this paper were spanwise-averaged for all cases (Bell, Plesniak & Mehta 1992). This was done by dividing the measurements obtained on a cross-plane grid into 'slices' through the mixing layer. The properties computed from each slice were then averaged with those obtained at other spanwise positions. In effect, the mixing-layer properties were averaged over 30–70 velocity profiles measured at the defined spanwise locations.

An error analysis, based on calibration accuracy and repeatability of measurements, indicates that mean streamwise velocity measurements with the cross-wire were accurate to within 3%, while mean cross-stream velocities were accurate to within 10%. Reynolds normal stress measurements were accurate to within 6%, and shear stresses were accurate to within 15–20%.

The measurements of U, W, and $\overline{u'w'}$ were corrected for mean streamwise velocity gradient ($\partial U/\partial Y$) effects (Bell & Mehta 1989*a*). In the vortex generator and corrugation cases, since relatively high values of $\partial U/\partial Z$ were encountered in addition, the measurements of V and $\overline{u'v'}$ were also corrected for shear effects. The streamwise component of mean vorticity ($\omega_x = \partial W/\partial Y - \partial V/\partial Z$) was computed using the central difference method. The overall circulation was found by taking the surface integral of the streamwise vorticity over the cross-flow plane with vorticity levels less than 20% of the maximum value being set to zero in order to provide immunity from 'noise'. The integration was applied across a rectangular 'box' on the measured grid that fully

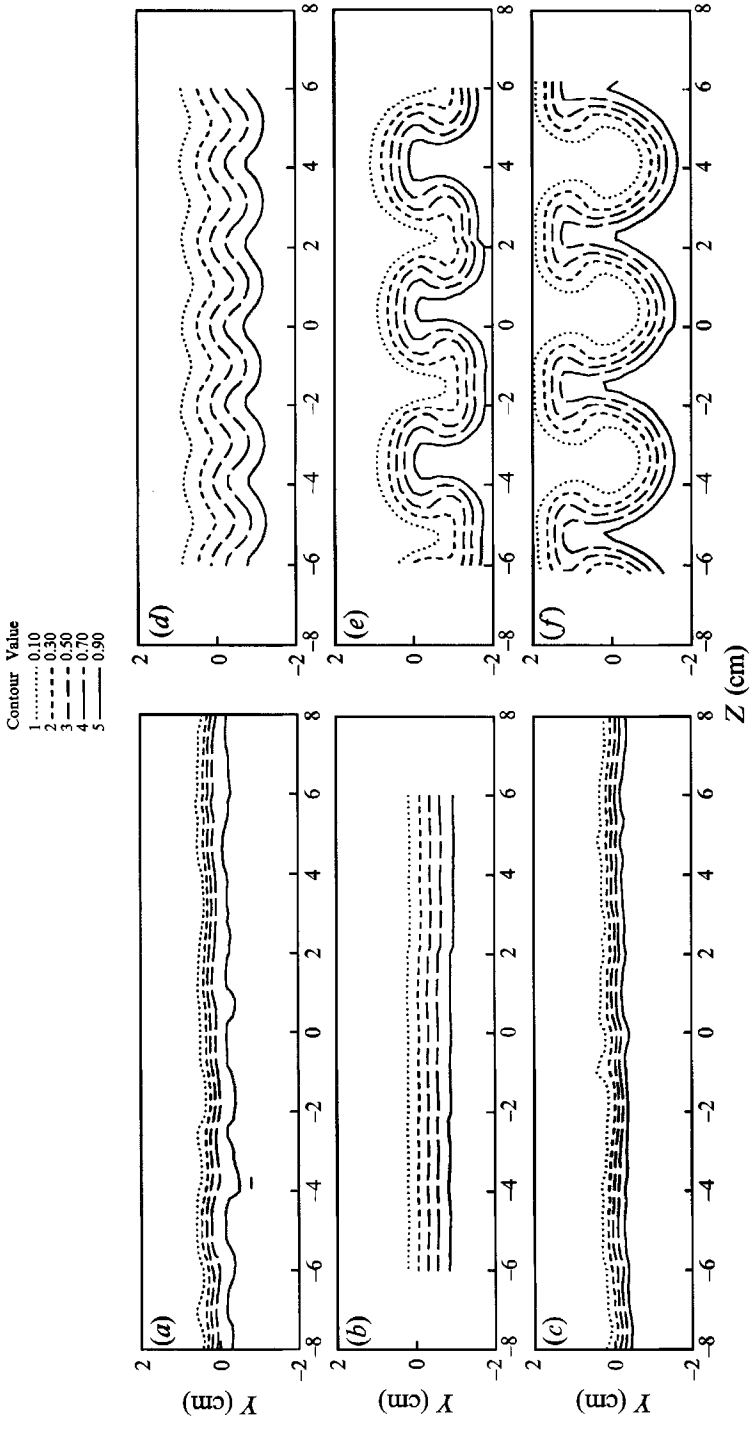

FIGURE 3. Mean streamwise velocity $[(U-U_2)/U_0]$ contours at $X \approx 17$ cm: (*a*) undisturbed, $X = 17$ cm; (*b*) tripped, $X = 17$ cm; (*c*) serration, $X = 15$ cm; (*d*) pegs, $X = 17$ cm; (*e*) vortex generators, $X = 17$ cm; (*f*) corrugation, $X = 14$ cm.

encompassed each identified vortex (that containing at least two closed vorticity contours with the spacing of the contour levels chosen to equal 10% of $(\Omega_x)_{max}$). The mean streamwise vorticity measurements were repeatable to within about 20% and the circulation measurements were repeatable to within about 25%.

3. Results and preliminary discussion

3.1. *Three-dimensional structure*

The measurements are first presented in the form of contour plots at two representative streamwise locations ($X \approx 17$ and 78 cm – the X distances were slightly lower for the serration (by 2 cm) and corrugation cases (by 3 cm) where the splitter plate trailing edge was extended). The locations of these stations in terms of the initial mixing-layer momentum thickness are given below in table 4. Wherever appropriate, results for the laminar (undisturbed boundary layers) and turbulent (tripped boundary layers) cases, without vorticity injection, are also included for comparison. All the data are normalized by the velocity difference across the mixing layer, $U_0 = U_1 - U_2$.

Contour plots of the mean streamwise velocity and vorticity, measured at $X \approx 17$ cm in the near-field region of the mixing layer, are presented in figures 3 and 4, respectively. The results highlight the considerable differences in the near-field evolution of the six cases. This is true even for the two cases (undisturbed and tripped) without vorticity injection (figures 3 and 4*a*, *b*). The velocity contours for the undisturbed case exhibit some random kinks caused by the presence of 'clusters' of streamwise vorticity (figure 4*a*). The streamwise vortices produce momentum transport in the cross-stream direction which results in the distorted mean velocity contours. The velocity contours for the tripped case, on the other hand, are almost straight and parallel, suggesting the absence of any organized, spatially stationary streamwise vorticity. This notion is confirmed by the vorticity measurements, which for the tripped case show levels lower than the undisturbed case by an order of magnitude, with no evidence of any organization (figure 4*b*).

The serration, pegs, vortex generators, and corrugations were all intended to produce a regular array of streamwise vortices in the mixing layer, as opposed to the irregular distribution present in the undisturbed case. This was achieved with varying degrees of success, as shown in figure 4. The serration appears to have a relatively small, if any, effect in organizing the vorticity distribution or changing its strength. In both the undisturbed and serration cases, the streamwise vortices appear to be organized in clusters, the locations of the clusters being determined by the locations of weak incoming disturbances (Bell & Mehta 1992). In both cases, the mean velocity contours (figure 3*a*, *c*) show the same pattern of random wrinkles. If anything, the streamwise vortices in the serration case seem to be having a smaller effect on the mixing layer – the wrinkles in the mean velocity contours appear weaker than those in the undisturbed case.

The perturbation provided by the other three mechanisms is clearly more effective at distorting the velocity contours, as shown in figure 3(*d*–*f*). A very regular distortion, which spans the whole mixing-layer width, is evident with the expected wavelengths of 2 cm for the peg case (reproducing the spacing between the pegs) and about 4 cm for the vortex generator and corrugation cases (following the 3.8 cm wavelength of the perturbations). The vortex generator and corrugation cases exhibit 'mushroom' shapes similar to those observed in previous flow visualization studies (Bernal & Roshko 1986; Lasheras & Choi 1988). This type of severe cross-stream distortion should significantly increase mixing between the two streams (Eckerle *et al.* 1992). The

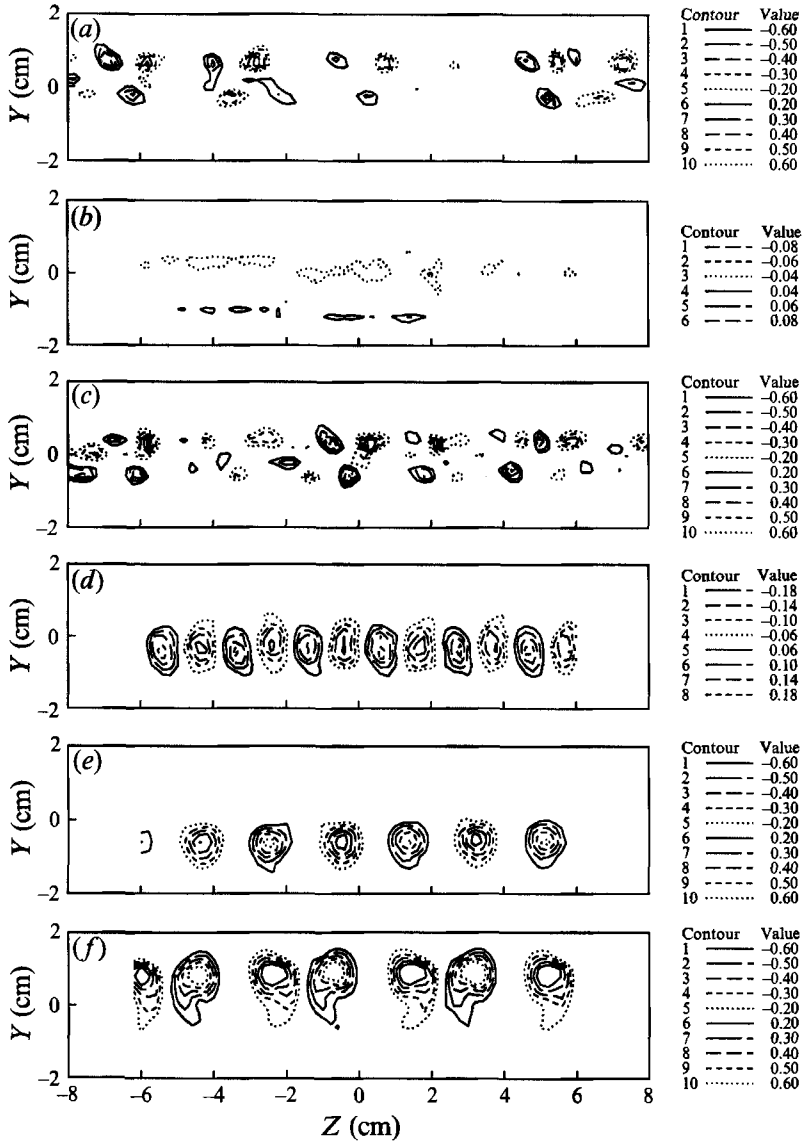

FIGURE 4. Mean streamwise vorticity (Ω_x/U_0, cm^{-1}) contours at $X \approx 17$ cm: (*a*) undisturbed, $X = 17$ cm; (*b*) tripped, $X \approx 17$ cm; (*c*) serration, $X = 15$ cm; (*d*) pegs, $X = 17$ cm; (*e*) vortex generators, $X = 17$ cm; (*f*) corrugation, $X = 14$ cm.

mean vorticity measurements (figure 4*d–f*) confirm that the distortion is the result of a regular array of streamwise vortices in the mixing layer. Although the peak vorticity levels in the peg case are somewhat lower than those in the undisturbed case, the regular distribution and larger scale result in a more distinct (sinusoidal) distortion of the mean velocity contours. The strengths of the vortices generated by the vortex generators and the corrugation are higher in comparison, and result in much stronger distortion of the mean velocity contours. In both the peg and vortex generator cases, the location of the row of vortices is biased towards the high-speed side of the mixing layer. This is to be expected since the perturbations were installed within the high-speed side boundary layer. In addition, the spacing between adjacent (opposite-signed)

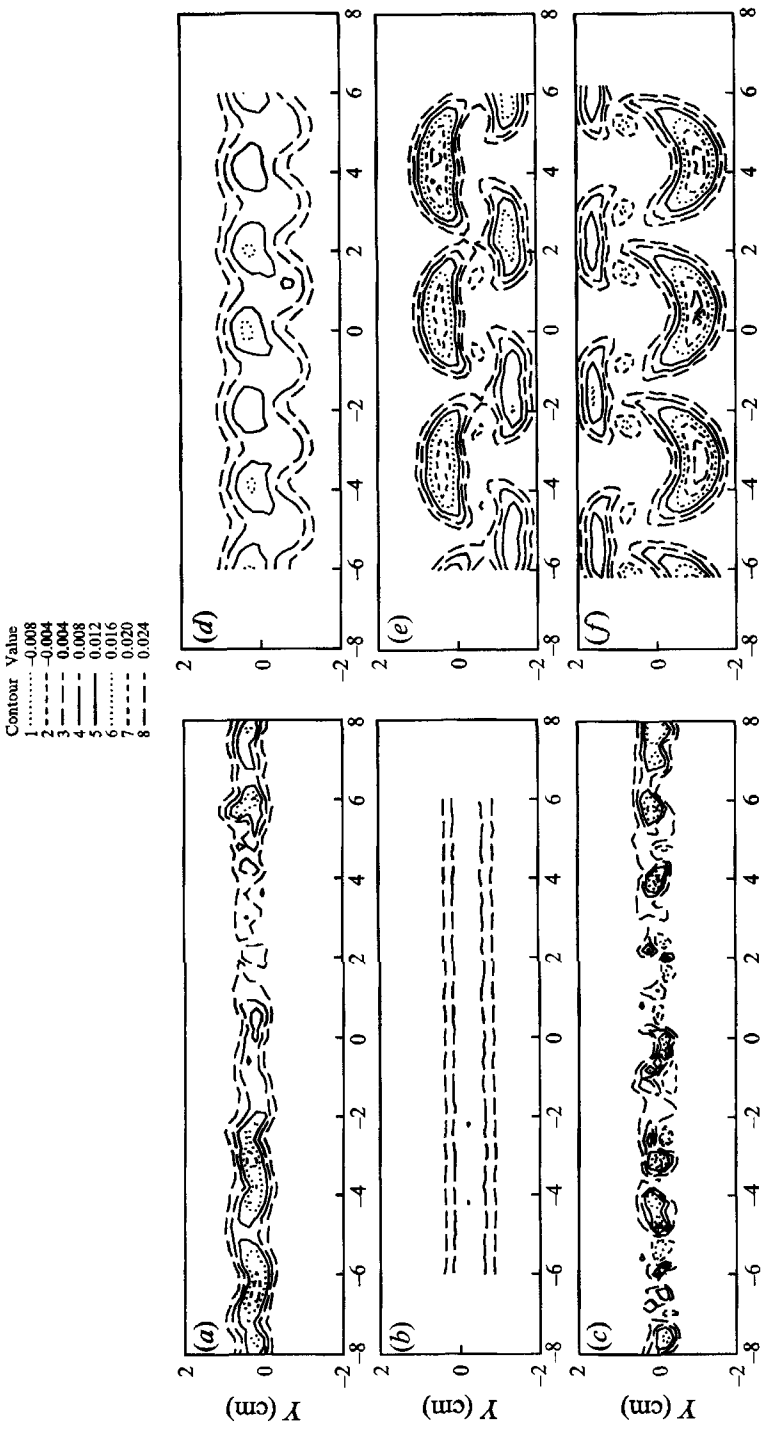

FIGURE 5. Primary shear stress $(\overline{u'v'}/U_0^2)$ contours at $X \approx 17$ cm: (*a*) undisturbed, $X = 17$ cm; (*b*) tripped, $X = 17$ cm; (*c*) serration, $X = 15$ cm; (*d*) pegs, $X = 17$ cm; (*e*) vortex generators, $X = 17$ cm; (*f*) corrugation, $X = 14$ cm.

vortices in these cases is constant and the mean velocity contours appear symmetric about the mixing-layer centreline. In contrast, in the corrugation case, the distance between pairs of vortices is greater than that between the vortices making up the pair. The vortex row is also biased towards the low-speed side and the mean velocity contours are not symmetric about the layer centreline. Note that the generation of vorticity in the peg and the vortex generator cases relies only on the high-speed stream whereas the vortex generation from the corrugation relies on both streams and some asymmetry is, therefore, not too surprising. As described above in §2, the streamwise vortices in the corrugation case result from the skewing (in opposing directions) of the boundary layers on the two sides of the splitter plate. Owing to the greater momentum of the high-speed side fluid, the resultant streamwise vortices are convected cross-stream towards the low-speed side and laterally towards the local trough, thus giving rise to the asymmetric distribution observed in figure 4(*f*). It is interesting to note that this type of asymmetric distribution of the streamwise vortices is also reproduced in temporal simulations using the vortex dynamics method (Ashurst & Meiburg 1988) and the direct numerical method (Rogers & Moser 1991) when the splitter plate wake is represented in the initial velocity profile.

The mean velocity contours presented in figure 3 reiterate the importance of spanwise-averaging of the data. Typical mixing-layer properties can have relatively large spanwise variations in this near-field region. For example, the relative standard deviation of the mixing-layer thickness varies from about 3% in the tripped case to about 50% in the corrugation case, with that in the undisturbed case being about 15%.

The distributions of the turbulence quantities in the mixing layer are also significantly affected by the imposed streamwise vorticity. Since the perturbations have qualitatively similar effects on all the Reynolds stresses, only the primary shear stress ($\overline{u'v'}$) results are presented here. The $\overline{u'v'}$ contours for all six cases at $X \approx 17$ cm are shown in figure 5(*a–f*). The distributions for the undisturbed and serration cases show an irregular distortion with isolated peaks, whereas that for the tripped case appears nominally two-dimensional. The peak shear stress levels for the undisturbed and serration cases are significantly higher than for the tripped case – this is the classically observed 'laminar overshoot'. The peg case also exhibits distorted shear stress contours, but in a regular sinusoidal form with a local peak at every crest location. The shear stress contours for the vortex generator and corrugation cases basically show isolated peaks distributed in a regular array. In all cases, the local peaks appear in regions where the velocity contours are crowded together (in the Y-direction) leading to stronger mean velocity gradients ($\partial U/\partial Y$), and hence higher $\overline{u'v'}$ production, through the $\overline{v'^2}\partial U/\partial Y$ term in the shear stress transport equation. Note also how the regions of negative $\partial U/\partial Y$ in the corrugation case (figure 3*f*) lead to the production of negative $\overline{u'v'}$ (figure 5*f*). In addition to $\partial U/\partial Y$, $\partial U/\partial Z$ and gradients of the secondary velocities (V and W) are also generated which affect the production of all the Reynolds stress components.

Some interesting changes in the mixing-layer structure are observed with increasing downstream distance, as seen in figures 6 and 7, which show the mean streamwise velocity and vorticity contours, respectively, at $X \approx 78$ cm. The velocity contours for the undisturbed and serration cases (figure 6*a*, *c*) appear very similar with a regular sinusoidal variation of about 5 cm wavelength. The regular spanwise variation is caused by the realignment of the clusters of mean streamwise vorticity into a single row of counter-rotating vortex pairs as seen in figure 7(*a*, *c*). The realignment of the vorticity is mainly caused by induced velocity effects – the vorticity is expected to continue to realign until an equilibrium state is achieved whereby it forms a single row of equally spaced counter-rotating pairs, with the strengths comparable. Note that the

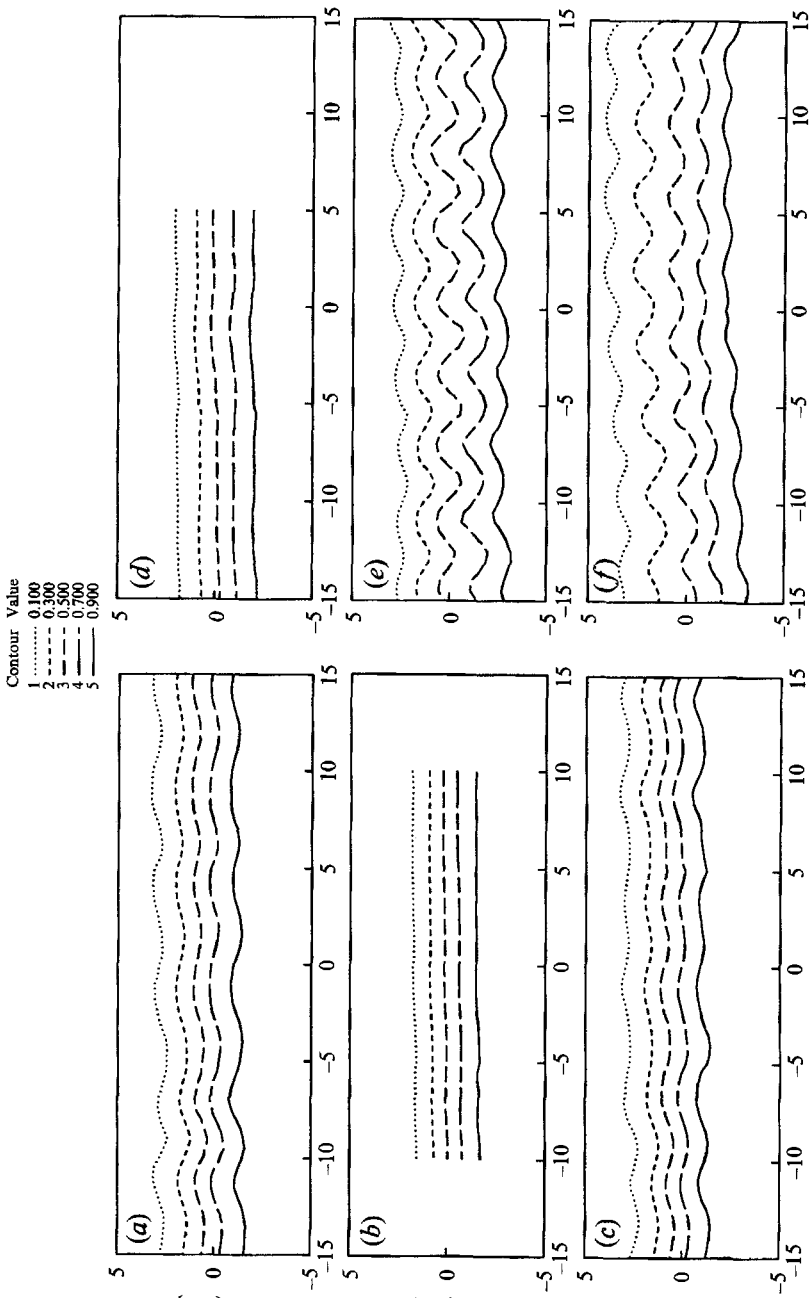

FIGURE 6. Mean streamwise velocity $[(U-U_2)/U_0]$ contours at $X \approx 78$ cm: (*a*) undisturbed, $X = 78$ cm; (*b*) tripped, $X = 78$ cm; (*c*) serration, $X = 76$ cm; (*d*) pegs, $X = 78$ cm; (*e*) vortex generators, $X = 78$ cm; (*f*) corrugation, $X = 75$ cm.

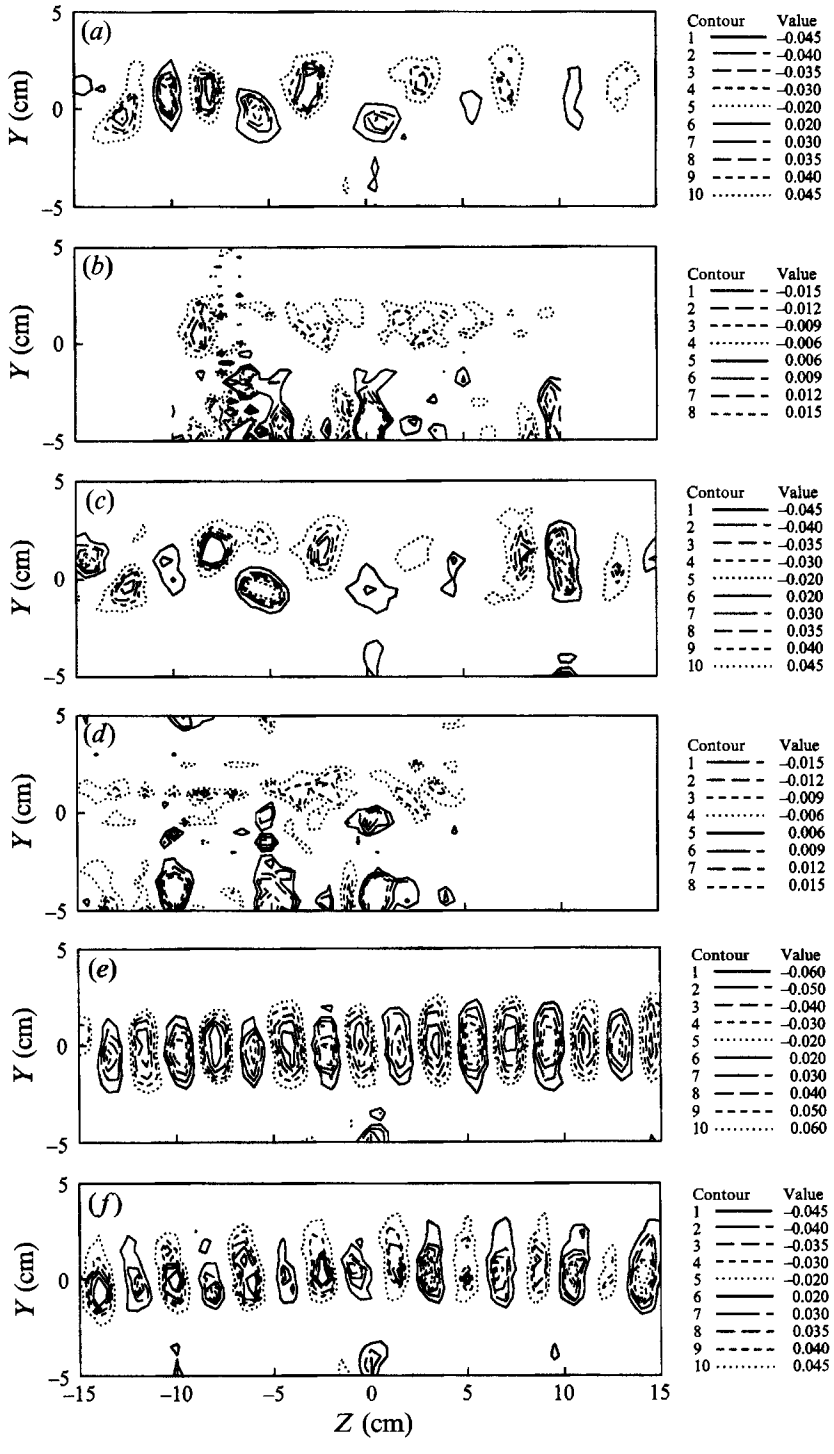

FIGURE 7. Mean streamwise vorticity (Ω_x/U_0, cm^{-1}) contours at $X \approx 78$ cm: (*a*) undisturbed, $X = 78$ cm; (*b*) tripped, $X = 78$ cm; (*c*) serration, $X = 76$ cm; (*d*) pegs, $X = 78$ cm; (*e*) vortex generators, $X = 78$ cm; (*f*) corrugation, $X = 75$ cm.

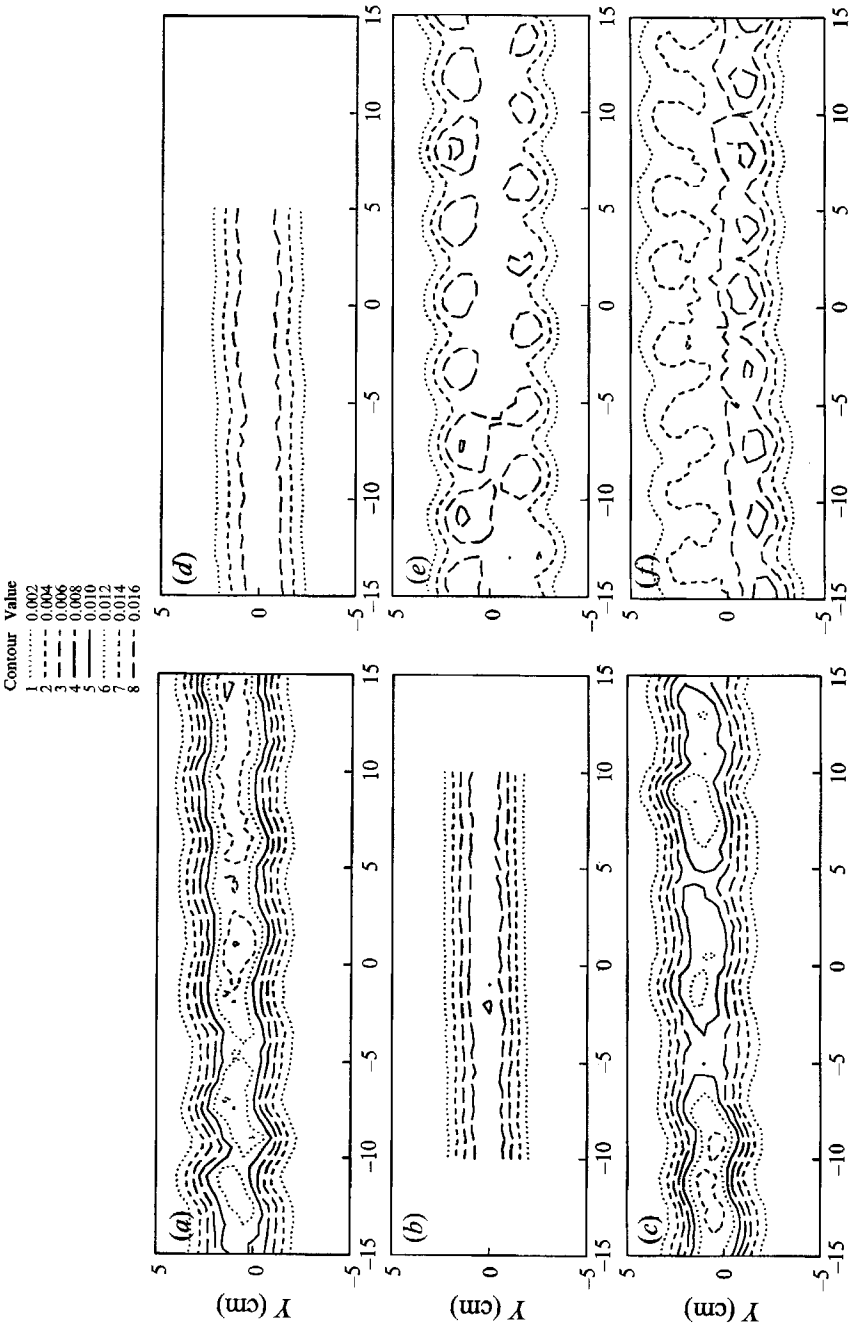

FIGURE 8. Primary shear stress $(\overline{u'v'}/U_0^2)$ contours at $X \approx 78$ cm: (*a*) undisturbed, $X = 78$ cm; (*b*) tripped, $X = 78$ cm; (*c*) serration, $X = 76$ cm; (*d*) pegs, $X = 78$ cm; (*e*) vortex generators, $X = 78$ cm; (*f*) corrugation, $X = 75$ cm.

distribution of the individual vortical structures and peak levels are very similar for the two cases. Also, the peak mean vorticity levels have decayed drastically with streamwise distance. With no spatially stationary vorticity present, the contours for the tripped case (figure 7*b*) continue to indicate a two-dimensional behaviour (figure 6*b*). Somewhat surprisingly, so do the results for the peg case (figure 6*d*), thus implying that the injected streamwise vorticity has decayed relatively quickly. This is confirmed by the mean streamwise vorticity results for this case (figure 7*d*) which show only very low levels, those comparable to the 'noise' in the measurement scheme. The streamwise vortices generated by the vortex generators and the corrugation exhibit a symmetric (unbiased) distribution with equal spacing between adjacent vortices. The peak levels of mean vorticity have again decayed in both cases with a slightly faster decay in the corrugation case (figure 7*e*, *f*). The regular distribution of the streamwise vortices has resulted in the very regular distortion of the mean velocity contours (figure 6*e*, *f*), which now takes the form of a sinusoidal wrinkle. Note that the wrinkle wavelength (~ 4 cm) is about the same as that observed at the upstream station ($X \approx 17$ cm). The amplitude of the wrinkle is slightly higher for the vortex generator case, as would be expected from the higher mean vorticity levels.

The primary shear stress contours at this station, presented in figure 8, reflect similar trends. The undisturbed and serration cases exhibit distorted contours, similar to the mean velocity contours, but with local peaks and higher shear stress levels than all the other cases. The contours for the tripped and peg cases appear almost straight and parallel, indicating a nominally two-dimensional turbulence structure. The vortex generator and corrugation cases still exhibit a severe, but very regular distortion, with local peaks symmetrically distributed.

By the measurement station at $X = 78$ cm, almost all the measured quantities for the serration case were found to be identical to those in the undisturbed case. Measurements at further downstream locations were, therefore, not obtained for this case. Although the serration had some near-field effects, it did not successfully trigger a regular array of streamwise vortices as had been expected based on Lasheras & Choi's (1988) results (obtained at a relatively low Reynolds number of $Re_\delta \approx 300$). The main reason for this failure was that, at the relatively high Reynolds numbers of the present study ($Re_\delta \approx 2.5 \times 10^4$), the regular perturbation produced by the serration had decayed almost completely by the time the flow reached the location of the first spanwise roll-up where amplification occurs. This was borne out by measurements of the mean streamwise velocity in the very near-field of the mixing layer (figure 9). The results clearly show how the regular perturbation introduced by the serration decays rapidly with streamwise distance such that the original signature is completely lost by the location of the first spanwise roll-up (at $X \approx 5$ cm, based Bell & Mehta's (1992) results for the undisturbed case). Huang & Ho (1990) also reported that relatively weak disturbances in the form of tape blocks were not effective in triggering the streamwise vortices in their mixing layer at high Reynolds number ($Re_\delta \approx 1.7 \times 10^4$).

Further downstream, the mean streamwise vorticity was found to decay monotonically in all cases such that the mixing layer appeared nominally two-dimensional at the last measurement station ($X \approx 250$ cm). Details of the mean streamwise vorticity evolution for all the cases are given in §3.3.

3.2. *Streamwise development of global properties*

Following Townsend (1976), the mixing-layer thickness, δ, is defined by fitting the mean streamwise velocity data to an error function profile shape:

$$U^* = \tfrac{1}{2}[1 + \mathrm{erf}(\zeta)], \tag{1}$$

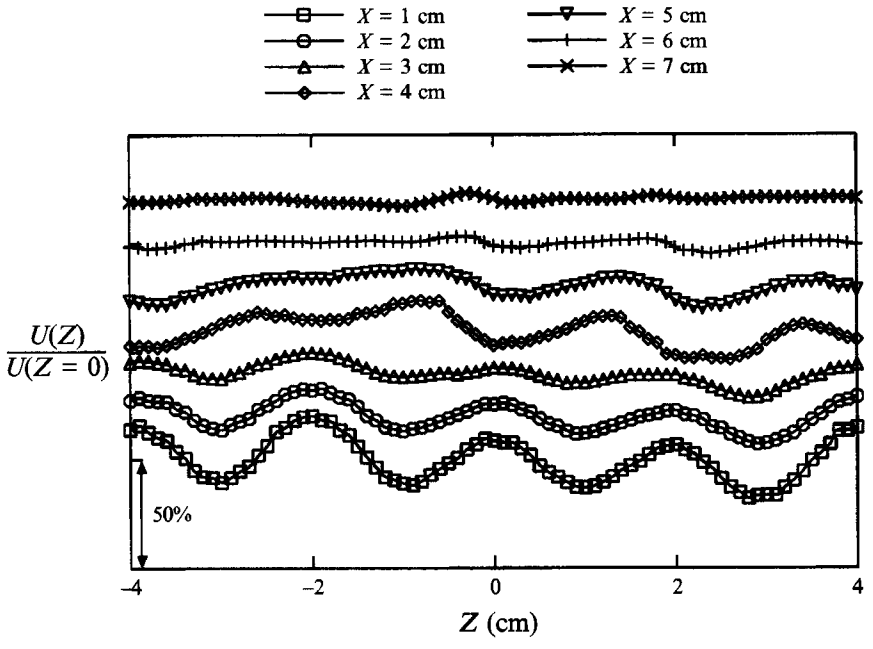

FIGURE 9. Spanwise variation of mean velocity (U) along the mixing-layer centreline ($Y = 0$) for the serration case.

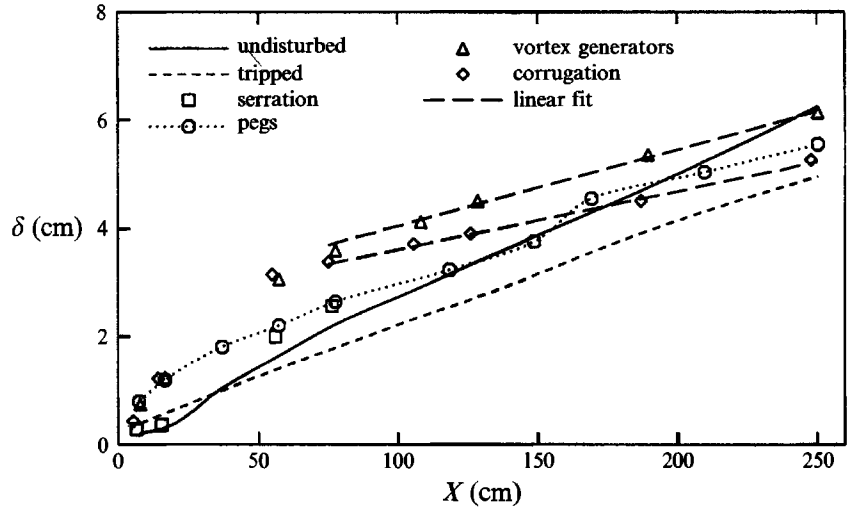

FIGURE 10. Streamwise development of mixing-layer thickness.

where $U^* = (U - U_2)/U_0$ and ζ is the normalized y-coordinate:

$$\zeta = (Y - Y_0)/\delta. \tag{2}$$

The values of δ and Y_0 are determined by optimizing the error function fit.

The streamwise development of the spanwise-averaged mixing-layer thickness is shown for all the cases in figure 10. We consider first the cases with untripped initial boundary layers, namely the undisturbed, serration, and peg cases. Note that the serration and undisturbed case thicknesses are nearly identical, reinforcing the

Case	$d\delta/dx$
Undisturbed	0.023
Tripped	0.019
Vortex generators	0.012
Corrugation	0.011
Brown & Roshko (1974)	0.023
Browand & Troutt (1985)	0.021

TABLE 2. Far-field growth rates

impression given in the contour plots that the effects of this perturbation are negligible. The perturbation introduced by the pegs clearly has a much larger effect. Based on the velocity contours in figure 3, it may seem surprising that the peg case (and not the corrugation) has the highest thickness at $X \approx 8$ cm, but note that figure 10 shows the spanwise-averaged (local) thickness, rather than the thickness of the spanwise-averaged layer. Near-field growth is also increased markedly, while the far-field growth remains nonlinear to the end of the measurement region, indicating that an asymptotic state is not achieved. The similarity between this growth profile and the stepwise growth observed in mixing layers subjected to periodic forcing (Oster & Wygnanski 1982) has prompted the suggestion that regular vortex shedding by the pegs is perhaps providing an excitation which locks-in the spanwise vortex pairing locations (J. Jimenez, private communication). It is interesting to note that the nonlinear behaviour starts at $X \approx 78$ cm, by which point about three spanwise vortex pairings should have occurred giving a spanwise vortex passage frequency of about 90 Hz (Bell & Mehta 1989*a*) and the estimated peg shedding frequency (based on a Strouhal number of 0.21) is about 100 Hz.

The far-field growth rate, determined by a least-squares fit to the thickness data between $X = 78$ cm and $X = 250$ cm, is given in table 2. The growth rates for the serration and peg cases are not tabulated since the serration case was not continued into the far-field region and the peg case exhibited a nonlinear growth, as discussed above. Also included in table 2, for reference, is the growth rate based on the relation suggested by Brown & Roshko (1974) for the vorticity thickness, δ_ω:

$$d\delta_\omega/dx = 0.16\lambda, \tag{3}$$

and that proposed by Browand & Troutt (1985) for the momentum thickness, θ:

$$d\theta/dx = 0.034\lambda, \tag{4}$$

where the relations, $\delta = \delta_\omega/\pi^{\frac{1}{2}}$ and $\delta = (2\pi)^{\frac{1}{2}}\theta$ are used for the conversion.

The growth rate of the undisturbed mixing layer is the same as that given by Brown & Roshko's (1974) relation (equation (3)) derived from a compilation of data obtained by several investigators. However, it is about 10% higher than that predicted by Browand & Troutt's (1985) relation (equation (4)) based on their own (single profile) measurements of two-stream mixing layers originating from laminar boundary layers. As discussed in §2, the present measurements were obtained on large cross-plane grids and then spanwise-averaged. Somewhat ironically, as shown in Bell *et al.* (1992), if the growth rate of the undisturbed case is evaluated from only the centreline ($Z = 0$) profiles, then a value of $d\delta/dx = 0.021$ is obtained, exactly the same as that given by Browand & Troutt's relation.

In the absence of vorticity injection, the growth rate of the mixing layer is clearly influenced by the state of the initial boundary layers. The asymptotic growth rate for

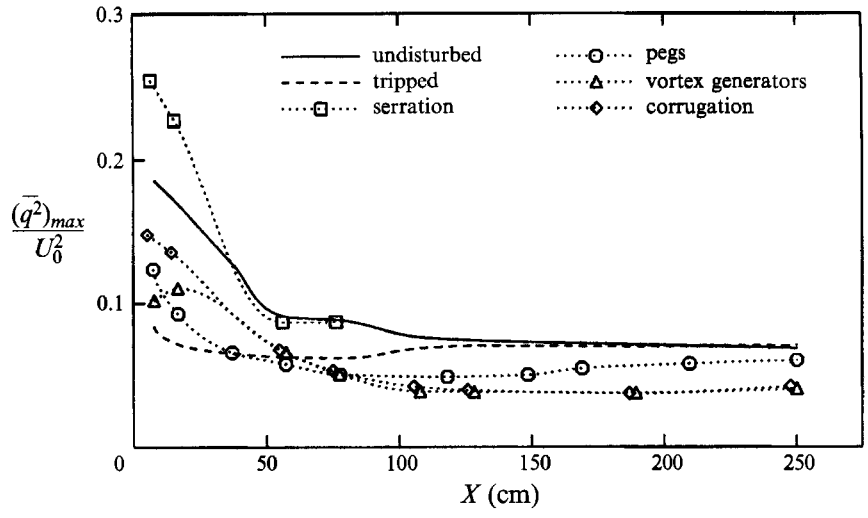

FIGURE 11. Streamwise development of maximum turbulent kinetic energy.

the tripped mixing layer is significantly lower (by about 25%) than that for the undisturbed case (table 2). It was previously hypothesized that the undisturbed case grew faster owing to extra entrainment provided by the streamwise vorticity (Bell & Mehta 1990), although the structure of the spanwise rollers in the two cases may also be affected, as discussed below in §4. The injection of streamwise vorticity into the tripped case was, therefore, expected to increase its growth rate by providing an additional source of entrainment. In this regard, the pegs, vortex generators and corrugation have substantially the same effects. The expected higher growth rate is achieved in the near-field ($X \leqslant 60$ cm), as clearly seen in figure 10. However, further downstream ($X \geqslant 100$ cm), the asymptotic linear growth rates for the vortex generator and corrugation cases are *reduced* significantly (by about 40%) over both the undisturbed and tripped cases. Despite the differences in the nature of the perturbations, the vortex generator and corrugation cases both grow at nearly the same rate.

Since the mixing-layer growth rates are so drastically affected by the perturbations at the origin, the Reynolds stress levels might be expected to show a comparable effect. This is indeed the case, as shown in figure 11, where the streamwise development of the spanwise-averaged peak turbulent kinetic energy $[(\overline{q^2})_{max}]$ is plotted. Actually, it is twice the turbulent kinetic energy since $\overline{q^2}$ is defined as, $\overline{q^2} = \overline{u'^2} + \overline{v'^2} + \overline{w'^2}$. Despite the relatively large difference in growth rates, both the undisturbed and tripped cases asymptote to about the same constant level of $(\overline{q^2})_{max}$ (≈ 0.07) beyond $X \approx 125$ cm. This asymptotic value agrees reasonably well with the data compiled by Rodi (1975) for two-stream mixing layers. The perturbed cases also achieve approximately constant levels in the far-field region, but lower than those for the cases without vorticity injection. The energy in the peg case levels-off at $(\overline{q^2})_{max} \approx 0.05$ in the region $X =$ 100–150 cm, but then exhibits an upward trend further downstream, perhaps indicating a recovery from the effects of the perturbation. The $(\overline{q^2})_{max}$ levels for the vortex generator and corrugation cases, on the other hand, do not show such obvious signs of a recovery from the lower constant level of about 0.04. In the near-field, the undisturbed case displays the classically observed 'overshoot' in turbulence intensity, before dropping down to the asymptotic level. The overshoot seen in the perturbed

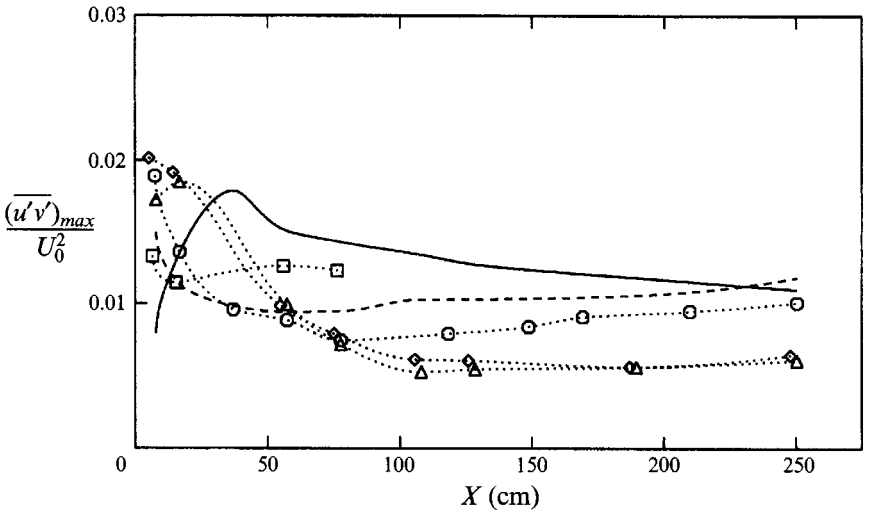

FIGURE 12. Streamwise development of maximum primary shear stress. For legend see figure 11.

cases is due to the generation of normal stresses, as the mixing layer is distorted by the strong streamwise vortices, thus producing high mean velocity gradients. In the undisturbed case, the overshoot is made up of very strong fluctuations at the Kelvin–Helmholtz frequency, while in the perturbed cases it is much more broadband. The slight overshoot in the tripped case is due to the effects of the splitter plate wake, which is somewhat stronger in this case compared to the undisturbed case (Mehta 1991).

The spanwise-averaged peak primary shear stress $[(\overline{u'v'})_{max}]$ levels are similarly affected (figure 12). The tripped case achieves a constant level of $(\overline{u'v'})_{max} \approx 0.011$ beyond $X \approx 100$ cm, and, by $X \approx 250$ cm, the undisturbed case has also reached a comparable level. The peg case slowly approaches a level which is only slightly lower (~ 0.010) than that of the two cases without vorticity injection. This behaviour further confirms that the peg case is certainly recovering from the effects of vorticity injection. The vortex generator and corrugation cases appear to asymptote to about the same constant level, but relatively early ($X \approx 100$ cm), and the level is significantly lower (~ 0.006), consistent with the lower growth rates, as further discussed below. The fact that the peak stress levels in the near-field are so different, even for cases which are otherwise comparable, such as the undisturbed and serration, is not really surprising. Plesniak, Bell & Mehta (1993) showed that even very small changes in initial conditions, such as those produced by swapping the high- and low-speed sides, can affect the peak Reynolds stress levels in the near-field region significantly.

In order to investigate whether the peak turbulent kinetic energy and shear stress have been affected proportionately by the various perturbations, their ratio, defined here as, $a_1 = (\overline{u'v'})_{max}/(\overline{q^2})_{max}$, is plotted in figure 13. Downstream of $X \approx 150$ cm, a_1 for all the cases has collapsed to within about 15% of the value, $a_1 = 0.16$ – a value of $a_1 = 0.15$ is normally observed in fully developed turbulent flows. The collapse of a_1 in the far-field region implies that $\overline{q^2}$ and $\overline{u'v'}$ are indeed affected proportionately and that the turbulence structure for all cases is perhaps similar. It is interesting that the vortex generator and corrugation cases exhibit more or less constant (and approximately equal) levels of a_1 throughout their development.

It is possible to relate approximately the peak level of primary shear stress, $(\overline{u'v'})_{max}$,

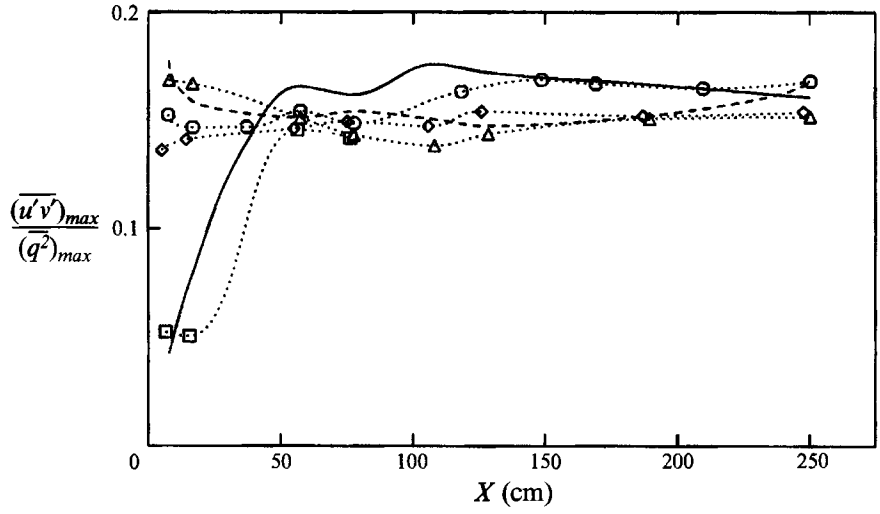

FIGURE 13. Streamwise development of turbulence structural parameter, a_1. For legend see figure 11.

$(\overline{u'v'})_{max}$	Undisturbed	Tripped	Vortex generators	Corrugation	High-speed	$\lambda = 0.54$
Measured	0.011	0.011	0.0061	0.0065	0.0071	0.0069
Calculated	0.013	0.010	0.0067	0.0060	0.0073	0.0089

TABLE 3. Measured and calculated $(\overline{u'v'})_{max}$

to the mixing-layer growth rate, $\mathrm{d}\delta/\mathrm{d}x$, for a given velocity ratio parameter, λ. The simplified relation for a two-dimensional, self-similar mixing layer that evolves from the analysis given by Townsend (1976), is:

$$-\frac{(\overline{u'v'})_{max}}{U_0^2} = 0.141 \frac{\mathrm{d}\delta}{\mathrm{d}x} \frac{1}{\lambda}. \tag{5}$$

This relationship (based on some crude assumptions) is used here only to infer details regarding the mixing-layer structure, and not as a prediction tool. The measured and calculated values of $(\overline{u'v'})_{max}$ for cases where linear growth and asymptotic values of the peak shear stress were obtained are compared in table 3.

The measured and calculated values of $(\overline{u'v'})_{max}$ in the tripped, vortex generator and corrugation cases agree to within $\pm 10\%$. The relatively poor agreement in the undisturbed case ($\sim 20\%$) suggests that this layer has not reached an equilibrium (self-similar) state. Indeed, we expect that self-similar plane mixing layers will be homogeneous in the Z-direction (Townsend 1976), and contour plots of this mixing layer (Bell & Mehta 1992) exhibit spanwise variations associated with the presence of spatially stationary streamwise vortices all the way up to the last station. Note that the predicted value of $(\overline{u'v'})_{max}$ is higher, and this, together with the lower growth rate of the tripped case, suggests that the undisturbed layer has an 'abnormally high' growth rate. Bell & Mehta (1990) attributed the higher growth rate to the presence of the spatially stationary streamwise vortices which supply additional entrainment. Since the streamwise vortices decay with streamwise distance, and since all the Reynolds stress

components (including $\overline{u'w'}$) achieved approximately constant (or near-zero) levels by the end of the measurement domain, Bell & Mehta hypothesized that the undisturbed mixing-layer growth rate would decrease further downstream. In fact, the turbulence structure of the undisturbed case is very similar to that of the tripped case by the last station and so it is expected that the undisturbed growth rate would eventually drop down to that of the tripped case. In all respects, the tripped case appears to have achieved the final asymptotic (self-similar) state in the present study. Furthermore, comparisons with some recent results from a direct numerical simulation of a mixing layer developing from turbulent velocity fields show that the tripped case growth rate and turbulence distributions are very similar to the ones computed in the self-similar region (Moser & Rogers 1992; Rogers & Moser 1993*b*). The simulation results also show that self-similarity is achieved faster when the initial conditions are turbulent (as opposed to laminar), in agreement with the present observations. Therefore, in the present study, the tripped case is regarded as the base case for comparisons with the perturbed cases.

One of the assumptions in the derivation of equation (5) is that the mean velocity profile of a self-similar mixing layer is well represented by an error function. So the invalidity of equation (5) could be due to a difference in velocity profile shapes. However, on examining the present data, it was found that the far-field velocity profiles for all cases were adequately represented by the error function. Another 'built-in' assumption is that the mixing layer does not have any additional entrainment mechanism which may contribute to the growth of the layer. As discussed above, we believe that the three-dimensionality in the undisturbed case, in the form of spatially stationary streamwise vortices, does precisely that. The validity of equation (5) may, therefore, be looked upon as an indicator of two-dimensionality (in the mean). In view of this, it is really surprising that the perturbed cases, which are more three-dimensional in the near-field, owing to the stronger injected streamwise vorticity, also satisfy equation (5). However, as shown below in §3.3, the stronger injected vorticity also decays faster and the perturbed cases therefore appear more two-dimensional in the far-field region ($X > 100$ cm) compared to the undisturbed case. In addition to the two-dimensionality, the perturbed cases also seem to satisfy some of the other conditions necessary for self-similarity, namely linear growth and nominally constant peak Reynolds stress levels, although the growth rates and peak stress levels are much lower than the corresponding values for the tripped case. Thus, these cases would seem to violate the principle of self-similarity, in that the mixing-layer far-field properties are manifestly dependent on initial conditions (Townsend 1976). However, a careful examination of the spanwise-averaged profiles plotted in similarity coordinates reveals that the perturbed cases may still be undergoing some readjustments. The primary shear stress profiles at the last four stations in the seemingly asymptotic region for the vortex generator and corrugation cases are shown in figures 14(*a*) and 14(*b*), respectively. The results for the vortex generator case clearly show a slow, but monotonic, increase in the peak shear stress levels as the profile becomes 'fuller' near the centreline. In the corrugation case, the peak levels do not vary as much, but the shape again changes, becoming more symmetric about the centreline. The question which then arises is with regard to the development distance required for these perturbed mixing layers to fully recover from the effects of the initial conditions. In the present facility, measurements downstream of $X = 250$ cm were found to be impractical owing to contamination from the sidewall boundary layers. In order to extend measurements farther downstream effectively, additional data were obtained for the corrugation case at different operating conditions.

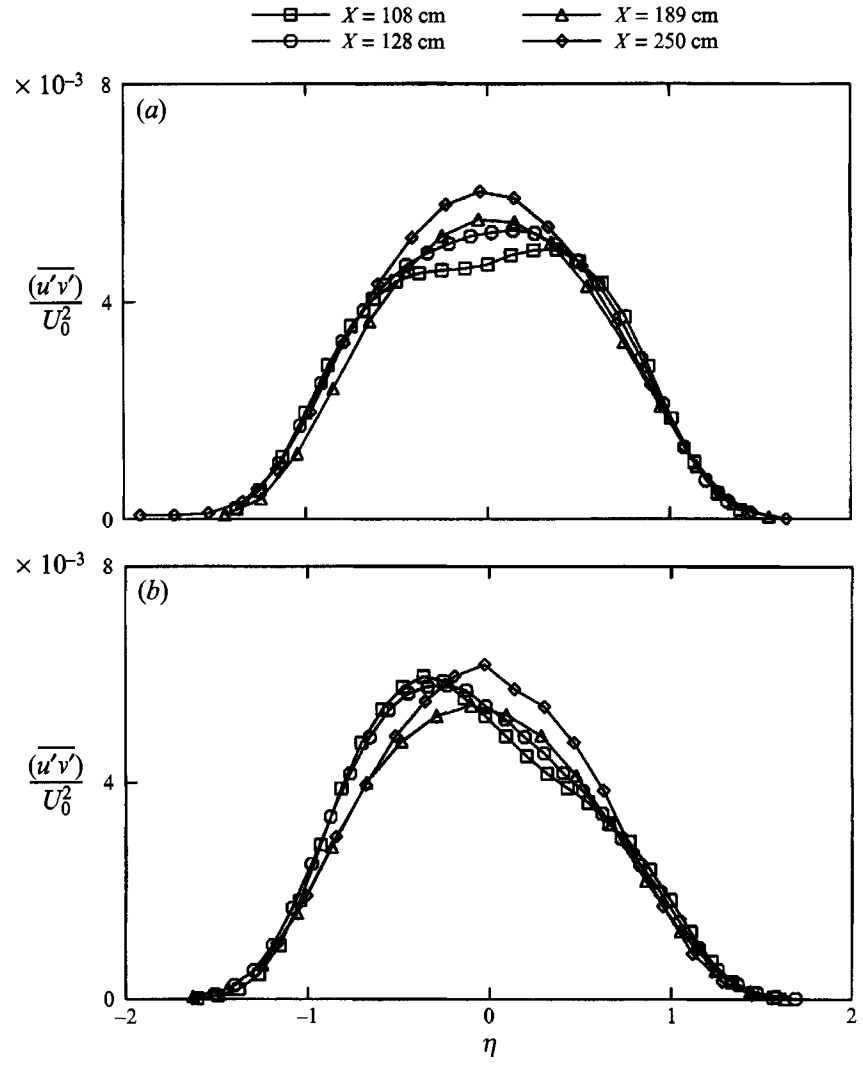

FIGURE 14. Primary shear stress ($\overline{u'v'}/U_0^2$) profiles in the far-field region: (*a*) vortex generators; (*b*) corrugation.

First, the flow velocity on both sides was doubled to produce a 'high-speed' case. Doubling the velocities doubles Re_x at the last station from 9.8×10^5 to 2.0×10^6. Data were obtained at the last three streamwise locations in order to determine the far-field turbulence levels and growth rate. The increased velocities resulted in about a 20% increase in growth rate, from $\mathrm{d}\delta/\mathrm{d}x = 0.011$ in the base corrugation case to $\mathrm{d}\delta/\mathrm{d}x = 0.013$, but this is still considerably lower than that of the tripped case ($\mathrm{d}\delta/\mathrm{d}x = 0.019$). The maximum shear stress also increased (by about 10%), such that the relationship given by equation (5) still holds well (table 3), thus suggesting that the streamwise vorticity in this mixing layer has also decayed relatively quickly. The results indicate that the far-field effect of the corrugations is reduced with increasing free-stream velocity. They also imply that the growth rate and peak Reynolds stress levels may continue to increase with Re_x, so that at sufficiently large Re_x (i.e. a sufficiently large distance downstream) a full recovery is achieved. It is quite clear though, that full

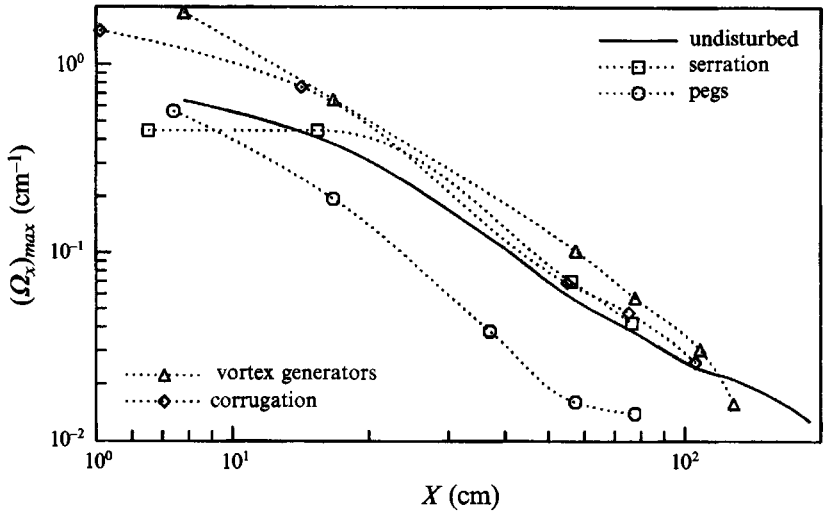

FIGURE 15. Streamwise development of peak mean streamwise vorticity.

recovery may take a very long streamwise distance to accomplish, probably too long to be relevant in most practical applications.

A second case was produced by increasing the high-speed side velocity from 15 m/s to 30 m/s, while maintaining the low-speed side velocity at 9 m/s, giving $\lambda = 0.54$ ($r = 0.33$). In this '$\lambda = 0.54$' case, the velocity difference was increased relative to the convection velocity with the expectation that more pairings of the spanwise structures will have occurred by a given streamwise location, thus making the mixing layer dynamically 'older' at that location. In this case, a higher growth rate ($\mathrm{d}\delta/\mathrm{d}x = 0.034$) was obtained, as expected for a higher velocity ratio, but the measured $(\overline{u'v'})_{max}$ was also increased to 0.0069. While this case displayed linear growth and constant Reynolds stresses, the measured level of $(\overline{u'v'})_{max}$ is about 30% lower than that predicted by equation (5), as shown in table 3. The lack of agreement indicates that this mixing layer may still contain some three-dimensionality, and, as discussed above, this may be responsible for extra entrainment, resulting in a higher growth rate for a given shear stress level. It is quite reasonable to expect that the three-dimensionality in a mixing layer is a function of the velocity difference across the layer. A higher velocity difference means a higher shear which leads to stronger spanwise vortices and hence more stretching in the braids. So this case, with stronger streamwise vortices, may take even longer to achieve an equilibrium state.

3.3. *Development of the mean streamwise vorticity*

In the time-averaged measurements obtained in this study, the most representative properties which assess the vortex strength are the peak mean streamwise vorticity and mean circulation. In the cases for which these quantities are measurable, their streamwise evolutions are presented in figures 15–17. The development of the peak mean streamwise vorticity, averaged over all vortices identified at a given station, is plotted on a log–log scale in figure 15. The vortex generator and corrugation cases have the highest initial mean vorticity levels, while those for the other three cases are comparable. Not surprisingly, the behaviour of the serration case is quite similar to that of the undisturbed case. Although the near-field decay is different for each case, in the region $X \approx 15$–100 cm the peak levels for all cases fall approximately along straight lines, indicating power-law-type decay rates. The peak mean vorticity in the

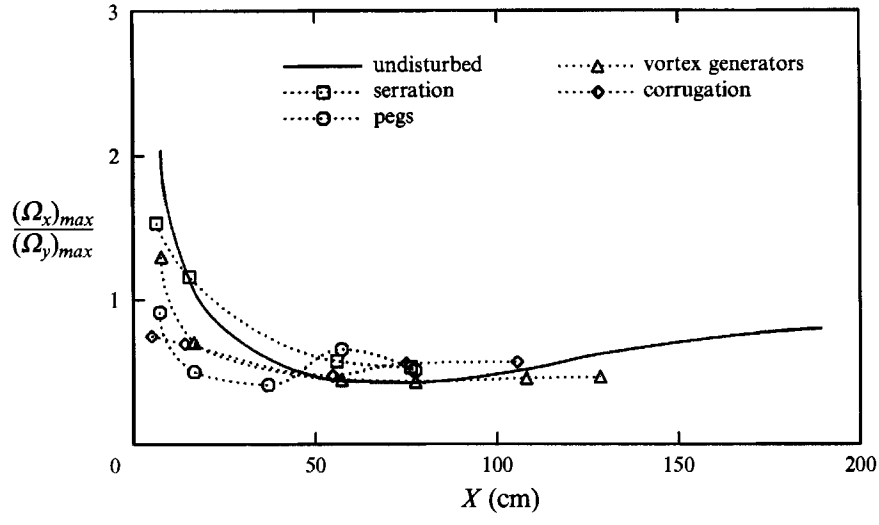

FIGURE 16. Streamwise development of streamwise to spanwise vorticity ratio.

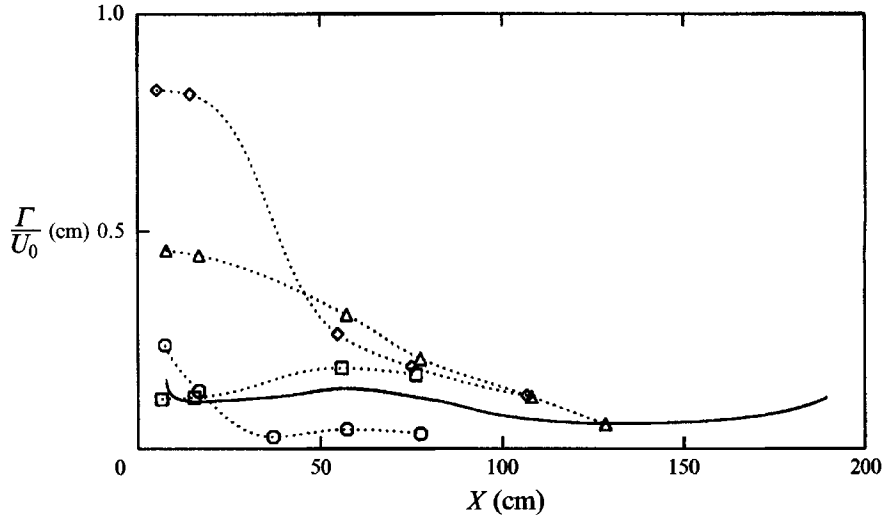

FIGURE 17. Streamwise development of average streamwise vortex circulation. For legend see figure 16.

undisturbed case decays as approximately $1/X^{1.5}$ while that in the vortex generator and corrugation cases decays somewhat faster ($1/X^{1.6}$), thus giving comparable levels in the three cases by $X \approx 100$ cm. Further downstream, the peak vorticity levels for the vortex generator and corrugation cases dropped to the point where they became comparable to the background noise. The highest vorticity decay rate is observed in the peg case ($1/X^{1.8}$), and since its initial levels are comparable to those in the undisturbed case, this results in relatively weak vorticity at $X = 78$ cm. It should be noted that these values only reflect the decay of the spatially stationary part of the secondary structure. It is possible that the structure is actually maintaining its strength, but 'meandering' with increasing amplitude as it moves downstream. Such vortex meander would decrease the mean vorticity measured at a given station. However, the balance of evidence suggests that most of the observed decay is real rather than an artifact of meander (Bell

& Mehta 1992; LeBoeuf & Mehta 1993). This view is consistent with the numerical simulation results which show that streamwise ('rib') vortices do not persist through to the self-similar region (Moser & Rogers 1992).

The rate of real decay is at least partly determined by the level of anisotropy $(\overline{v'^2}-\overline{w'^2})$ in the turbulence field, which is responsible for the production or maintenance of streamwise vorticity (Bell & Mehta 1992). Although the pegs produce a very strong and regular perturbation in the mixing layer, the vorticity appears to decay the fastest. The main reason for this effect is that the pegs, apart from producing the streamwise vorticity, also make the laminar boundary layer on the high-speed side transitional. The overall result is that the peak levels of $\overline{v'^2}$ and $\overline{w'^2}$ are comparable in the near-field region of the peg case, thus reducing the level of anisotropy. This means that production of vorticity due to anisotropy is small and, hence, decay of the vortices occurs faster.

The secondary vortex structure is idealized to exist mostly in the braid region at an angle to the mean flow. Thus, the structure contains both streamwise and cross-stream vorticity. Assuming that streamwise velocity gradients are small compared to spanwise gradients, it is possible to estimate the cross-stream vorticity, $\Omega_y = (\partial U/\partial Z) - (\partial W/\partial X)$, by neglecting the $\partial W/\partial X$ term. To some extent, the ratio of streamwise to cross-stream vorticity, Ω_x/Ω_y, reflects the angle which the secondary structure makes with the mean flow. Note that Ω_y also has a contribution from the undulation of the spanwise vortices, so that Ω_x/Ω_y is also a measure of the spanwise vortex distortion associated with a given amount of streamwise vorticity. The peak cross-stream vorticity at each measurement station was estimated, and the streamwise evolution of Ω_x/Ω_y is plotted for each case with significant secondary structure in figure 16. In the undisturbed and serration cases, the developing secondary structure only gradually begins to kink the mixing layer, resulting in a very high Ω_x/Ω_y ratio initially. In the other three cases, the high level of spanwise distortion imposed by the perturbations produces a much lower Ω_x/Ω_y ratio. Further downstream ($X > 50$ cm), Ω_x/Ω_y collapses to approximately the same level of about 0.5 for all cases, suggesting that the secondary structure is behaving in a similar fashion in all cases, despite differences in the generation mechanisms and near-field behaviour.

Plots of the mean streamwise circulation per vortex (figure 17) show very different behaviour for the various cases. The undisturbed case vortex circulation shows a very slow decrease, with a small intermediate peak at $X \approx 60$ cm. Once again, the serration case behaves similarly. In contrast, the vortex generator case shows a relatively fast linear decay and by $X \approx 125$ cm, its level is comparable to that of the naturally occurring vortices. In the corrugation case, the circulation at the first two stations is quite high; it then drops rapidly to a level close to that of the vortex generator case. This result is surprising, since the peak vorticity of the corrugation case at the first station is lower than that for the vortex generator case. Evidently, the corrugations produce relatively diffuse, large-scale streamwise vortices which the mixing layer cannot support, and these decay rapidly. Thus, the circulation decay in the corrugation case does not follow the linear decrease observed in the vortex generator case. By $X \approx 100$ cm, the circulation levels for the vortex generator and corrugation cases are comparable to those for the undisturbed case and they continue to decrease further downstream. The peg case displays features common to the undisturbed and serration cases on the one hand, and to the vortex generator and corrugation cases on the other. The strong vortices with relatively high circulation which are initially present quickly lose strength and an approximately constant level is achieved downstream of $X \approx$ 30 cm. The impression is that the imposed vorticity has dropped to a level at which it

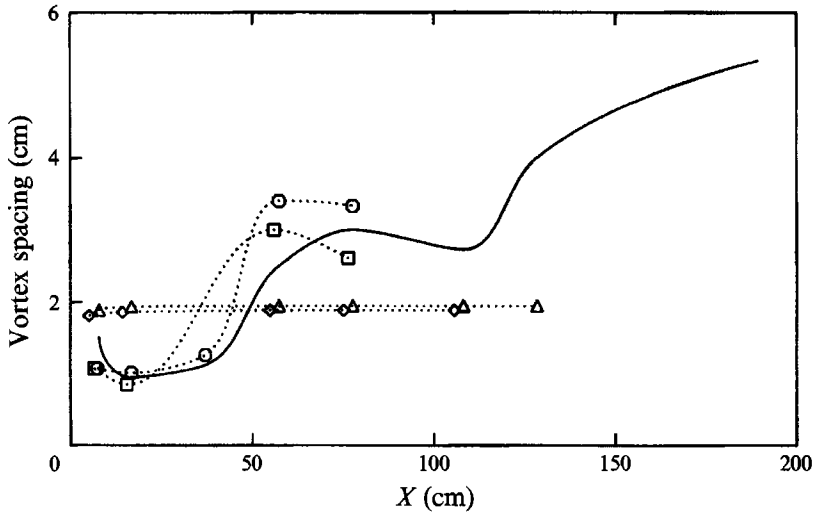

FIGURE 18. Streamwise development of vortex spacing. For legend see figure 16.

can be 'naturally' supported by the mixing-layer structure. Note the small peak at $X \approx 60$ cm, similar to the one in the undisturbed and serration cases.

The mean spacing of the streamwise vortices is calculated by dividing the spanwise extent of the measurement domain by the number of vortices detected at each station. The vortex spacing in the undisturbed, serration and peg cases increases in a step-wise fashion, scaling approximately as the mixing-layer vorticity thickness (figure 18). Since the first increase in spacing at $X \approx 50$ cm occurs approximately at the same location as the peak in circulation (figure 17), Bell & Mehta (1992) proposed that at least one mechanism for the increase in spacing is vortex amalgamation. Previous experimental investigations have shown that the scale change in the streamwise vortices occurs during the pairing of the spanwise rollers (Jimenez, Cogollos & Bernal 1985; Bell & Mehta 1992; Huang & Ho 1990), although a scale change is not observed at every spanwise vortex pairing location (Bell & Mehta 1992). The simulation results of Rogers & Moser (1993*a*) show that the details of the scale change are dependent on the amplitudes of the initial three-dimensional disturbances. The spacing for the vortex generator and corrugation cases, on the other hand, is constant within the measurement domain. This may simply be due to the fact that the injected vortices are of equal strength and spacing, unlike the naturally occurring structures, and remain that way so there is no tendency for self-induced motion. An irregular spanwise distribution and induced motion are necessary for the identified mechanisms (vortex amalgamations and annihilation) which can lead to a change in the scale, and hence spacing, of the streamwise vortical structures (Bell & Mehta 1992; Rogers & Moser 1993*a*). It is worth noting, that for the maintenance of a constant spanwise spacing, the regularity of the array will become increasingly important as the initial spacing between the injected vortices is reduced.

The behaviour of the peg case is interesting in this regard. Despite the injection of a regular vortex array (figure 4*d*), the peg case vorticity shows a scale change similar to the undisturbed case. This is probably related to the spanwise uniformity of the streamwise vorticity. Note that while the streamwise vortices in the vortex generator and corrugation cases remain similar in strength across the span as the layer develops, this is obviously not true in the peg case (figures 4*d–f* and 7*d–f*). In fact, it was found

that the vorticity levels in the peg case became non-uniform by the measurement station at $X = 37$ cm (Bell & Mehta 1989*a*), immediately before the jump in spacing occurs (figure 18). The non-uniformity of the vortex strengths leads to cross-stream movement of the vortices owing to mutual induction, and hence, to a spanwise scale change as discussed above. The main difference between the peg case and the vortex generator and corrugation cases is that the initial boundary layers in the peg case were not tripped, although as discussed above, the high-speed side boundary layer was probably made transitional through the effects of the pegs. Therefore, complete transition of the flow occurs in the mixing layer and this is not likely to occur uniformly across the span. As a result, the anisotropy parameter should also be expected to be non-uniform across the span and this would result in a non-uniform decay, as discussed above.

4. Further discussion

One of the most important and interesting results from the present study is the effect of the perturbations on the mixing-layer growth rate. Most of the growth of a mixing layer occurs owing to entrainment during the pairing process of the nominally two-dimensional spanwise vortical structures (Winant & Browand 1974; Sandham *et al.* 1988). The entrainment is in the form of engulfment of fluid by the large-scale spanwise vortices as they pair. The naturally occurring streamwise vorticity in the undisturbed case first appears in the regions of maximum extensional strain, in the braids. The streamwise and spanwise structures become interlaced in such a way that, in flow-visualization studies, it appears that the only effect of the streamwise structure on the spanwise vortices is to produce a regular, gentle undulation in the latter (Lasheras *et al.* 1986). Therefore, the entrainment due to the spanwise structures proceeds undisturbed; total growth may in fact be enhanced by the additional entrainment in the braids owing to the secondary structure. However, the relatively strong injected streamwise vorticity in the vortex generator and corrugation cases must be expected to affect the coherence of the spanwise structures, based on the gross distortions in the mean velocity contours (figure 2*e*, *f*). It is conceivable that less fluid would be engulfed if the coherence of the spanwise structures were reduced, thus making them more three-dimensional. It is also possible that the pairing rate of the spanwise structures is affected since weaker, less coherent spanwise structures would induce lower velocities upon each other. Thus, vortex pairing would occur at a slower rate. In fact, in a recent simulation of a temporally-developing mixing layer originating from turbulent velocity fields, Moser & Rogers (1992) showed that the spanwise structures do not appear to pair in the self-similar region. Rather, adjacent spanwise structures exchange vorticity without the large-scale co-rotation and consequent engulfment of free-stream fluid, leading to a reduced growth rate. The spanwise structures in this region were not as well defined as in laminar and transitional mixing layers (Rogers & Moser 1991) and their spanwise coherence was also reduced – obviously, these basic differences in the spanwise structures must also be partly responsible for the difference in growth rates between the undisturbed and tripped cases. So it is proposed here that the injected streamwise vorticity reduces entrainment by the spanwise structures, including engulfment during pairing and perhaps the pairing rate as well. In the near-field, additional entrainment by the secondary structure more than makes up for this deficit. However, entrainment due to the streamwise vortices decreases much faster than the spanwise structure recovery, so the overall entrainment rate is reduced, and hence the growth rate of the mixing layer drops.

Case	θ_0 (cm)	$X\lambda/\theta_0$ at $X \approx 8$ cm	$X\lambda/\theta_0$ at $X \approx 17$ cm	$X\lambda/\theta_0$ at $X \approx 78$ cm	$X\lambda/\theta_0$ at $X \approx 250$ cm
Undisturbed	0.056	36	76	348	1116
Tripped	0.081	25	53	241	772
Serration	0.054	37	79	361	1158
Pegs	0.173	12	25	113	361
Vortex generators	0.149	14	29	131	420
Corrugation	0.108	19	39	181	579

TABLE 4. Estimated initial mixing layer momentum thickness and non-dimensionalized streamwise distances

In terms of the development distance (to self-similarity) of a mixing layer, it has often been suggested that the appropriate lengthscale is the initial momentum thickness of the layer (θ_0). Bradshaw (1966) found that a single-stream mixing layer achieved self-similarity in a distance equivalent to $1000\theta_0$ for both, a tripped and untripped initial boundary layer, a result which has often been confirmed since. Ho & Huerre's (1984) compilation of peak turbulence level measurements, which included Bradshaw's results and two-stream mixing layer ($\lambda = 0.7$) data of Browand & Latigo (1979), showed that an asymptotic level was reached at $X\lambda/\theta_0 \approx 625$ (based on $X\lambda/\lambda_n = 20$ in their figure 17). Browand & Troutt (1985) found that their two-stream mixing-layer growth rates exhibited good collapse beyond $X\lambda/\theta_0 \approx 400$–$500$ for (untripped) layers with $\lambda = 0.41$–0.695. However, there is some doubt as to the universality of these correlations for all two-stream mixing layers, in particular for layers with a relatively low λ. For example, the two-stream mixing layers ($\lambda = 0.37$) studied by Mehta & Westphal (1986) appeared to achieve self-similarity in a distance equivalent to $X\lambda/\theta_0 \approx 70$. On the other hand, the tripped case ($\lambda = 0.25$) discussed here achieved it in $X\lambda/\theta_0 \approx 300$, while the undisturbed case with the same velocity ratio is expected to reach self-similarity beyond $X\lambda/\theta_0 \approx 1100$, as discussed above in §3.2 and by Bell & Mehta (1990). Apart from these effects of initial conditions on the development distance, some effect of velocity ratio is also expected since, as λ decreases, the splitter plate wake begins to play an important, and lasting, role in the mixing-layer development (Mehta 1991). Since there appears to be a lack of correlation, even for these relatively 'simple' two-stream mixing layers, one would not expect such a scaling to work for the perturbed layers in the present case, where the structure of the mixing layer is drastically altered.

In the present study, the initial momentum thickness was not measured directly. The estimated values, based on the assumption that all the mixing layers grow at the same rate upstream of the first measurement station at $X \approx 8$ cm, are given in table 4. Also included in the table are the equivalent distances (in terms of λ/θ_0) of the two representative locations ($X \approx 17$ and 78 cm) and those of the first ($X \approx 8$ cm) and last measurement stations ($X \approx 250$ cm).

The maximum $X\lambda/\theta_0$ values for the peg, vortex generator and corrugation cases are all lower than 1100, beyond which the undisturbed case is expected to achieve full self-similarity. They are also low compared to that given by Ho & Huerre's (1984) correlation, but lie within the band proposed by Browand & Troutt (1985). They are all higher, however, than $X\lambda/\theta_0 = 300$, the value at which the tripped case becomes self-similar. It is worth noting that the peg case which has the lowest $X\lambda/\theta_0$, shows a faster recovery in the maximum Reynolds stress results compared to the vortex generator and corrugation cases. So it is quite clear that for the development distance of two-stream mixing layers, a simple scaling based on the initial momentum thickness

and velocity ratio is not likely to be very successful, in general. A parameter that accounts for the initial structure of the mixing layer, in terms of the mean three-dimensionality perhaps, would have to be included if the mixing layer development distance is to be predicted accurately.

5. Conclusions

The effects due to four types of added perturbations on the three-dimensional structure of a plane mixing layer have been investigated. This study arose out of an attempt to understand the role which the streamwise vortical structure played in the observed differences in growth rates between mixing layers with laminar and turbulent initial boundary layers. A second objective was to reliably trigger or inject the streamwise structure in a mixing layer at relatively high Reynolds numbers so that it could be more easily studied, especially with regard to mixing-layer control applications. Previous studies on the effects of perturbations were restricted to the near-field region of low-Reynolds-number mixing layers.

The present results clearly show that the structure and growth of a turbulent mixing layer can be effectively controlled by imposing a relatively strong streamwise vortical structure at the origin. It was expected that vorticity injection would increase mixing-layer growth owing to extra entrainment for the streamwise structures and this was indeed observed in the near-field region. However, the far-field growth rate of these mixing layers is drastically reduced over the cases without vorticity injection and this is one of the most intriguing results of the present study. It is conjectured that the injection of relatively strong vorticity at the origin leads to reduced growth in the far field by breaking up the spanwise structures, making them more three-dimensional and reducing entrainment during pairing, and perhaps the pairing rate as well. In the near field, this effect is compensated for by increased entrainment from the streamwise structures, but this contribution is lost in the far field, where the streamwise structures have decayed.

In the region of reduced growth, these perturbed mixing layers seem to achieve an equilibrium state such that the peak Reynolds stress levels are reduced proportionately to the growth rate. This result is perhaps more important from the fundamental point of view, since it raises the possibility that mixing layers achieve different asymptotic states determined by the initial conditions, as suggested by George (1989). However, the balance of evidence in the present study suggests that these layers are recovering towards a (universal) self-similar state. The results for the peg case (with weaker injected vorticity) show some obvious signs of recovery, and the fact that the growth rate and peak shear stress levels for the corrugation case increase with Re_x suggest that this case should also recover eventually. However, the distance required for full recovery is not easily predicted, and it can be relatively long, probably too long for it to be relevant in most practical applications.

With respect to the second objective, the present study shows that relatively simple and weak perturbation mechanisms, such as the serration, will not always trigger a regular array of streamwise vortices, despite the success of this mechanism in low-Reynolds-number ($Re_\delta \approx 300$) water-channel experiments (Lasheras & Choi 1988). In the high-Reynolds-number conditions typically encountered in practical aerodynamics, the perturbation produced by a serration is likely to decay before reaching the point where amplification occurs (after the first spanwise vortex roll-up). Strong perturbations (compared to those naturally occurring), on the other hand, produce a very well-defined secondary vortex structure even at the higher Reynolds numbers achieved

in the present study. The injection of strong vorticity leads to an increased growth rate and increased mixing capabilities in the near-field region which would be beneficial in many combustion-type applications.

Both the naturally occurring and artificially imposed streamwise structures behave similarly in the mixing layer, in that they organize into a single row of equally spaced structures, whose peak vorticity then follows a log-law-type decay. One significant difference is noted, however, in that the vorticity injected in the vortex generator and corrugation cases does not show the spanwise scale change and circulation jump observed in the other cases. The main reason for the lack of scale change is that the uniform array of injected streamwise vortices remains uniform, although the peak mean vorticity decays with downstream distance. In this context, the behaviour of the peg case is especially interesting. Although a strong (regular) streamwise vortex structure is imposed in this case, a spanwise scale change is observed, as is nonlinear growth in the far-field. The nonlinear growth is attributed to forcing of the spanwise vortex pairings by vortex shedding from the pegs. The spanwise scale change is attributed to the non-uniform decay of the streamwise vortices owing to non-uniform transition in the mixing layer. Once the non-uniform array of streamwise vortices is created, the spanwise scale appears to increase in the same way as for the undisturbed case (through vortex amalgamation).

This work was supported by and conducted in the Fluid Mechanics Laboratory, NASA Ames Research Center under NASA Grant NCC-2-55. J.H.B. was also supported by the Center for Turbulence Research, NASA Ames/Stanford University during some phases of the project. We are grateful to Drs R. D. Moser and M. M. Rogers for many helpful discussions and also for reviewing a draft of this paper.

REFERENCES

ASHURST, W. T. & MEIBURG, E. 1988 Three-dimensional shear layers via vortex dynamics. *J. Fluid Mech.* **189**, 87–115.

BELL, J. H. & MEHTA, R. D. 1989*a* Three-dimensional structure of plane mixing layers. *JIAA Rep.* TR-90. Dept of Aeronautics and Astronautics, Stanford University.

BELL, J. H. & MEHTA, R. D. 1989*b* Design and calibration of the mixing layer wind tunnel. *JIAA Rep.* TR-89. Dept of Aeronautics and Astronautics, Stanford University.

BELL, J. H. & MEHTA, R. D. 1990 Development of a two-stream mixing layer with tripped and untripped boundary layers. *AIAA J.* **28**, 2034–2042.

BELL, J. H. & MEHTA, R. D. 1992 Measurements of the streamwise vortical structures in a plane mixing layer. *J. Fluid Mech.* **239**, 213–248.

BELL, J. H., PLESNIAK, M. W. & MEHTA, R. D. 1992 Spanwise averaging of plane mixing layer properties. *AIAA J.* **30**, 835–837.

BERNAL, L. P. & ROSHKO, A. 1986 Streamwise vortex structure in plane mixing layers. *J. Fluid Mech.* **170**, 499–525.

BRADSHAW, P. 1966 The effect of initial conditions on the developments of a free shear layer. *J. Fluid Mech.* **26**, 225–236.

BREIDENTHAL, R. 1980 Response of plane shear layers and wakes to strong three-dimensional disturbances. *Phys. Fluids* A **23**, 1929–1934.

BROWAND, F. K. & LATIGO, B. O. 1979 Growth of the two-dimensional mixing layer from a turbulent and nonturbulent boundary layer. *Phys. Fluids* A **22**, 1011–1019.

BROWAND, F. K. & TROUTT, T. R. 1985 The turbulent mixing layer: geometry of large vortices. *J. Fluid Mech.* **158**, 489–509.

BROWN, G. L. & ROSHKO, A. 1974 On density effects and large structure in turbulent mixing layers. *J. Fluid Mech.* **64**, 775–816.

ECKERLE, W. A., SHEIBANI, H. & AWAD, J. 1992 Experimental measurement of the vortex development downstream of a lobed mixer. *Trans. ASME* J: *Engng Gas Turbines & Power* **114**, 63–71.

GEORGE, W. K. 1989 The self-preservation of turbulent flows and its relation to initial conditions and coherent structure. In: *Advances in Turbulence* (ed. R. Arndt & W. K. George), pp. 75–125. New York: Hemisphere.

HO, C.-M. & HUERRE, P. 1984 Perturbed free shear layers. *Ann. Rev. Fluid Mech.* **16**, 365–424.

HUANG, L.-S. & HO, C.-M. 1990 Small-scale transition in a plane mixing layer. *J. Fluid Mech.* **210**, 475–500.

JIMENEZ, J. 1983 A spanwise structure in the plane mixing layer. *J. Fluid Mech.* **132**, 319–326.

JIMENEZ, J., COGOLLOS, M. & BERNAL, L. P. 1985 A perspective view of the plane mixing layer. *J. Fluid Mech.* **152**, 125–143.

KONRAD, J. H. 1976 An experimental investigation of mixing in two-dimensional turbulent shear flows with applications to diffusion-limited chemical reactions. *Project SQUID Tech. Rep.* CIT-8-PU; and PhD thesis, California Institute of Technology, 1977.

LASHERAS, J. C., CHO, J. S. & MAXWORTHY, T. 1986 On the origin and evolution of streamwise vortical structures in a plane, free shear layer. *J. Fluid Mech.* **172**, 231–258.

LASHERAS, J. C. & CHOI, H. 1988 Three-dimensional instability of a plane free shear layer: an experimental study of the formation and evolution of streamwise vortices. *J. Fluid Mech.* **189**, 53–86.

LEBOEUF, R. L. & MEHTA, R. D. 1993 Streamwise vortex meander in a plane mixing layer. *Phys. Fluids* A **5**, 1983–1991.

MEHTA, R. D. & WESTPHAL, R. V. 1986 Near-field turbulence properties of single- and two-stream plane mixing layers. *Exps Fluids* **4**, 257–266.

MEHTA, R. D. 1991 Effect of velocity ratio on plane mixing layer development: influence of the splitter plate wake. *Exps Fluids* **10**, 194–204.

MOSER, R. D. & ROGERS, M. M. 1992 Coherent structures in a simulated turbulent mixing layer. *IUTAM Symposium on Eddy Structure Identification in Free Turbulent Shear Flows, Oct 12–14, Poitiers, France.*

NYGAARD, K. J. & GLEZER, A. 1990 Core instability of the spanwise vortices in a plane mixing layer. *Phys. Fluids* A **2**, 461–463.

NYGAARD, K. J. & GLEZER, A. 1991 Evolution of streamwise vortices and generation of small-scale motion in a plane mixing layer. *J. Fluid Mech.* **231**, 257–301.

OSTER, D. & WYGNANSKI, I. J. 1982 The forced mixing layer between parallel streams. *J. Fluid Mech.* **123**, 91–130.

PIERREHUMBERT, R. T. & WIDNALL, S. E. 1982 The two- and three-dimensional instabilities of a spatially periodic shear layer. *J. Fluid Mech.* **114**, 59–82.

PLESNIAK, M. W., BELL, J. H. & MEHTA, R. D. 1993 Effects of small changes in initial conditions on mixing layer three-dimensionality. *Exps Fluids* **14**, 286–288.

RODI, W. 1975 A review of experimental data of uniform density free turbulent boundary layers. In *Studies in Convection* (ed. B. E. Launder), vol. 1, pp. 79–165, Academic.

ROGERS, M. M. & MOSER, R. D. 1991 The three-dimensional evolution of a plane mixing layer. Part 1. The Kelvin–Helmholtz roll-up. *NASA Tech. Mem.* 103856, September.

ROGERS, M. M. & MOSER, R. D. 1993*a* Spanwise scale selection in plane mixing layers. *J. Fluid Mech.* **247**, 321–337.

ROGERS, M. M. & MOSER, R. D. 1993*b* Direct simulation of a self-similar turbulent mixing layer. Submitted to *Phys. Fluids* A.

SANDHAM *et al.* 1988 Scalar entrainment in the mixing layer. *Proc. Summer Program, Center for Turbulence Research, Stanford University/NASA Ames Research Center*, pp. 69–76.

TOWNSEND, A. A. 1976 *Structure of Turbulent Shear Flow* (2nd edn). Cambridge University Press.

WINANT, C. D. & BROWAND, F. K. 1974 Vortex pairing: the mechanism of turbulent mixing layer growth at moderate Reynolds number. *J. Fluid Mech.* **63**, 237–255.